atmosphere

MDPI

Article

Modification of Fraser's Method for the Atmospheric CO_2 Mass Estimation by Using Satellite Data

Marco Pellegrini, Arash Aghakhani, Alessandro Guzzini * and Cesare Saccani

Department of Industrial Engineering, University of Bologna, 40136 Bologna, Italy; marco.pellegrini3@unibo.it (M.P.); arash.aghakhani2@unibo.it (A.A.); cesare.saccani@unibo.it (C.S.)
* Correspondence: alessandro.guzzini2@unibo.it

Abstract: One of the most critical greenhouse gases in the atmosphere is carbon dioxide (CO_2) due to its long-lasting and negative impact on climate change. The global atmospheric monthly mean CO_2 concentration is currently greater than 410 ppm which has changed dramatically since the industrial era. To choose suitable climate change mitigation and adaptation strategies it is necessary to define carbon dioxide mass distribution and global atmospheric carbon dioxide mass. The available method to estimate the global atmospheric CO_2 mass was proposed in 1980. In this study, to increase the accuracy of the available method, various observation platforms such as ground-based stations, ground-based tall towers, aircrafts, balloons, ships, and satellites are compared to define the best available observations, considering the temporal and spatial resolution. In the method proposed in this study, satellite observations (OCO2 data), from January 2019 to December 2021, are used to estimate atmospheric CO_2 mass. The global atmospheric CO_2 mass is estimated around 3.24×10^{15} kg in 2021. For the sake of comparison, global atmospheric CO_2 mass was estimated by Fraser's method using NOAA data for the mentioned study period. The proposed methodology in this study estimated slightly greater amounts of CO_2 in comparison to Fraser's method. This comparison resulted in 1.23% and 0.15% maximum and average difference, respectively, between the proposed method and Fraser's method. The proposed method can be used to estimate the required capacity of systems for carbon capturing and can be applied to smaller districts to find the most critical locations in the world to plan for climate change mitigation and adaptation.

Keywords: climate change; CO_2 concentration; climate change mitigation and adaptation; global atmospheric CO_2 mass; satellite data; OCO2

check for updates

Citation: Pellegrini, M.; Aghakhani, A.; Guzzini, A.; Saccani, C. Modification of Fraser's Method for the Atmospheric CO_2 Mass Estimation by Using Satellite Data. *Atmosphere* **2022**, *13*, 866. https://doi.org/10.3390/atmos13060866

Academic Editors: Adrianos Retalis, Vasiliki Assimakopoulos and Kyriaki-Maria Fameli

Received: 18 March 2022
Accepted: 21 May 2022
Published: 25 May 2022

Publisher's Note: MDPI stays neutral with regard to jurisdictional claims in published maps and institutional affiliations.

Copyright: © 2022 by the authors. Licensee MDPI, Basel, Switzerland. This article is an open access article distributed under the terms and conditions of the Creative Commons Attribution (CC BY) license (https://creativecommons.org/licenses/by/4.0/).

1. Introduction

Most of the literature agrees that greenhouse gases (GHGs) trap heat in the atmosphere and lead to global warming. One of the most critical GHGs is carbon dioxide (CO_2) which has attracted more attention than other GHGs due to its long-lasting presence in the atmosphere and negative impact on climate change. Furthermore, always increasing data would suggest that CO_2 concentration increases year after year. If 20 parts per million (ppm) was assumed based on high accuracy Antarctic ice-core records in 6000 Before Common Era (BCE) [1], more than ten times greater concentrations, i.e., up to around 281 ppm, were recorded during the Industrial Revolution between the 17th and the 18th centuries [2,3]. The global monthly mean CO_2 concentration is currently greater than 410 ppm, according to the National Oceanic and Atmospheric Administration (NOAA) website [4]. However, no simple correlation exists between global warming and available CO_2 concentration data. For this purpose, new CO_2 indexes should be introduced for the investigation of global warming problems. In fact, CO_2 concentration results from a complex balance between sources and sinks, such as, for example, anthropogenic activities and natural phenomena [5–7]. Therefore, many parameters must be considered, as shown in Table A2 in the Appendix A section.

However, despite the efforts to measure CO_2 concentration, the CO_2 mass calculation approach is inadequate. For instance, a preliminary estimation of about 7.15×10^{11} tons was reported in 1980 [8], while a more recent publication of the Global Carbon Budget in 2019 estimates an amount up to 8.60×10^{11} tons [9]. Therefore, 1.45×10^{11} tons of CO_2 seem to have been emitted in approximately 39 years, resulting in a mean annual positive flux to the atmosphere of 3.7 Gton/year (=$1.45 \times 10^{11}/39$). The annual growth rate in the atmospheric CO_2 mass was calculated from the concentration data reported by Dlugokencky and Tans [4], i.e., from the Global Greenhouse Gas Reference Network (GGGRN) that currently consists of 84 active sites in 37 countries. The complete GGGRN sites' list is reported in Table A3 in the Appendix A section. Despite the number of GGGRN sites increasing through the years with a maximum number of active sites up to 116 in 2011 (see Figure A1 in the Appendix A), the currently active 85 observatory sites appear insufficient to estimate the global CO_2 mass.

The first improvement in CO_2 mass estimation would be using data from more datasets and not limited to the one currently used. In fact, according to Jiang and Yung [10], many CO_2 datasets exist even if not included in the algorithms used for mass estimation. The list of existing surface-based and aircraft-based CO_2 concentration datasets is reported below:

Ground-based CO_2 concentration observations:

- The Earth System Research Laboratory of the National Oceanic and Atmospheric Administration (NOAA ESRL) [11];
- Total Carbon Column Observing Network (TCCON) [12].

Airborne based CO_2 concentration observations:

- The Earth System Research Laboratory of the National Oceanic and Atmospheric Administration (NOAA ESRL) [11];
- Comprehensive Observation Network for Trace Gases by Airliner (CONTRAIL) [13];
- Intercontinental Chemical Transport Experiment-North America (INTEX-NA) [14];
- High-performance Instrumented Airborne Platform for Environmental Research Pole-to-Pole Observations (HIPPO) [15];
- In-Service Aircraft for a Global Observing System (IAGOS) [16];
- Carbon in Arctic Reservoirs Vulnerability Experiment (CARVE) [17].

In addition to ground-based sites and airborne observation, data sets from ships can be acquired using research ships or commercial ones. For example, the NOAA National Centers for Environmental Information (NCEI) hosts a data management project, the Ocean Carbon Data System (OCADS), where data from deep and shallow waters are recorded to analyze CO_2 fluxes between the atmosphere and oceans. The following list includes ship-based observation under the OCADS project:

- Ships Of Opportunity Program (SOOP) Data [18];
- Global Surface pCO_2 (LDEO) [19].

In addition, there are atmospheric CO_2 concentration data sets generated in the open ocean sites using a moored autonomous system [20].

Although many algorithms exist at the present state of the art to measure CO_2 fluxes and concentration, they are too complex to give an answer to several research and industrial questions, limiting their potential applications. To give an accurate estimation and location of CO_2 mass amount through the use of simple algorithms is a research gap to be filled. For this purpose, i.e., to apply simple algorithms avoiding the use of state-of-the-art algorithms, big data for CO_2 are required. Since it is not economically possible to build new measuring sites around the world, the elaboration of the data coming from satellites is the best alternative. Particularly, the advantages and the challenges of CO_2 satellites monitoring for climate governance and for applications at national/regional, megacity and point source levels was already reviewed by [21]. For this purpose, the following satellite datasets can be considered for CO_2 concentration observations:

- The Orbiting Carbon Observatory-2 (OCO-3) [22];
- The Orbiting Carbon Observatory-2 (OCO-2) [23];

- The Greenhouse Gases Observing Satellite (GOSAT) [24];
- Thermal Emission Sounder (TES), measurement instrument installed on Aura satellite by NASA [25];
- Atmospheric InfraRed Sounder-Aqua satellite (AIRS) [26];
- The Infrared Atmospheric Sounding Interferometer (IASI) is an instrument flown on METOP satellite [27];
- The Atmospheric Chemistry Experiment (ACE) SciSat [28];
- The scanning imaging absorption spectrometer for atmospheric cartography (SCIAMACHY) onboard the Environmental Satellite (ENVISAT) [29];
- Other satellite missions are launched or will be launched in the future, such as Tansat, Carbonsat, MERLIN, Sentinel-5p, MicroCarb, and ASCENDS [3], which would increase the amount of available information.

Since more and more data will be available in the future from satellites, a new methodology for the atmospheric CO_2 mass estimation is described in the paper. To the best knowledge of the authors there has not been any study that uses solely satellite data to calculate global atmospheric CO_2 mass; however, there are some studies based on satellite data and simulation such as the atmospheric chemical transport model. In particular, the proposed approach ensures the estimation of the global mass but also the analysis of the atmospheric CO_2 mass variation in a specific location. Therefore, the new method makes it possible to perform a comparative analysis of the atmospheric CO_2 mass for different locations and time periods. The results of the proposed method can be used to estimate the required capacity of systems for carbon capturing based on the CO_2 mass. In addition, since the methodology is based on the division of the Earth's surface into smaller cells using satellite resolution it can be applied to smaller districts to find the most critical locations in the world to plan properly for climate change mitigation and adaptation.

The purpose of this paper is to validate a model using the best available observation platforms considering the resolution, coverage, and accuracy of the data to define the global atmospheric carbon dioxide mass regarding the mass distribution on the Earth with higher precision in comparison to the Fraser method. Since satellites were considered as input for the methodology, the validation of their data with respect to other platforms introduced in the Materials and Method section, i.e., ground-based stations, airborne and ships observations, is reported in the Results and Discussion sections. Finally, the new methodology for atmospheric CO_2 mass described in the Materials and Method section is validated with state-of-the-art values and discussed in the Results and Discussion section.

2. Materials and Method

2.1. Simplified Fraser's Method for the Calculation of CO_2 Atmospheric Mass

According to Fraser et al. [8], the global atmospheric carbon content was 7.15×10^{14} kg in 1980. The authors suggest Figure 1 as a schematic representation of the complex procedure which was used in [11] to estimate the global atmospheric carbon dioxide mass. The validation of the proposed methodology can be performed by comparing the results using the following steps. As shown, the first step is the calculation of the number of dry air moles (block c) in the atmosphere by dividing the global atmospheric mass of dry air (block a) by dry air mean molecular weight (block b) according to Equation (1):

$$\mathrm{Air}_{\mathrm{dry,mol}} = \frac{\mathrm{Air}_{\mathrm{dry,mass}}}{\mathrm{Air}_{\mathrm{dry,mw}}} \quad (1)$$

where:
$\mathrm{Air}_{\mathrm{dry,mol}}$ = Dry air moles (mol)
$\mathrm{Air}_{\mathrm{dry,mass}}$ = Global atmospheric mass of dry air (kg), that is 5.12×10^{18} kg;
$\mathrm{Air}_{\mathrm{dry,mw}}$ = Dry air mean molecular weight (kg/mol), that is 0.02897 kg/mol.

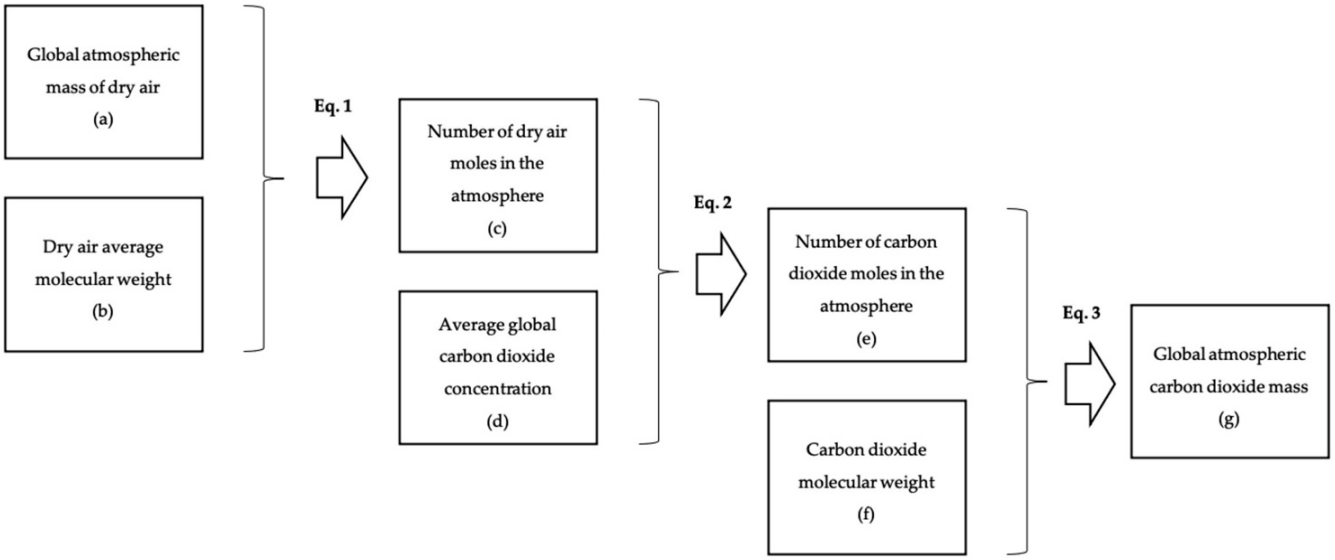

Figure 1. Building blocks for the global atmospheric carbon dioxide content calculation. Letters (**a**–**g**) are used to label the blocks in order to simplify mentioning the steps in the text.

In the second step, the number of CO_2 moles in the atmosphere is calculated (block e). For this purpose, the average global CO_2 concentration (block d) is multiplied by the number of dry air moles (block c) according to Equation (2):

$$CO_{2,mol} = CO_{2,con,avg,vol} \times Air_{dry,mol} \times 10^{-6} \quad (2)$$

where:
$CO_{2,mol}$ = CO_2 moles (mol)
$CO_{2,con,avg,mol}$ = Average global CO_2 concentration (ppm_v—part per million by volume)

The average global CO_2 concentration is calculated as the ratio between the CO_2 and the dry air as in Equation (3):

$$CO_{2,con,avg,vol} = \frac{CO_{2,vol}}{Air_{dry,vol}} \times 10^{6} \quad (3)$$

where:
$CO_{2,vol}$ = The volume of carbon dioxide (m^3)
$Air_{dry,vol}$ = The volume of dry air (m^3)

Since the desired parameter is the number of CO_2 moles, Equation (3) is manipulated through the ideal gas law to obtain Equation (4), then Equation (2) is achieved by manipulating Equation (4):

$$CO_{2,con,avg,vol} = \frac{CO_{2,mol}}{Air_{dry,mol}} \times 10^{6} \quad (4)$$

The last step is the calculation of the global atmospheric CO_2 mass (block g). The value is calculated by Equation (5) as the product between the number of CO_2 moles in the atmosphere (block e) and the CO_2 molecular weight (block f).

$$CO_{2,gac} = CO_{2,mol} \times CO_{2,mw} \quad (5)$$

where:
$CO_{2,gac}$ = The global atmospheric carbon dioxide content (kg)
$CO_{2,mw}$ = CO_2 molecular weight (kg), that is 44.01×10^{-3} kg/kmol.

Equation (5) is elaborated with the use of Equation (2) and Equation (1) to obtain Equation (6):

$$CO_{2,gac} = CO_{2,con,avg,vol} \times \frac{Air_{dry,mass}}{Air_{dry,mw}} \times CO_{2,mw} \times 10^{-6} \quad (6)$$

2.2. Data Sources for the Comparison of Existing Platforms for CO_2 Concentration's Measurement

Fraser's study used only 21 sites to calibrate the proposed model for CO_2 atmospheric concentration. However, through the years, more platforms have been established to measure CO_2 concentration, such as ground-based platforms (including ground-based stations and tall towers), aircraft, balloons, ships and satellite-based observations.

Ground-based measurement is a fixed-space measurement of CO_2 in a specific location on the earth. In addition to the earth coordinates (latitude and longitude), the elevation of the sampling vessel, i.e., the height regarding the level of the sea, is also fixed. Ground-based stations are research stations located at remote sites such as, but not limited to, islands, mountains, and coasts, although, some of them are located within a short distance from cities to assess the urban greenhouse gas emission. The selection of the sites is justified since the air samples taken at these locations would be easier to be integrate in global transport models. The Mauna Loa observatory site, located on the north flank of Mauna Loa Volcano in the main island of Hawaii (19.54° N, 155.58° W, 3397 m above the sea level (a.s.l.)) was the first station where the CO_2 concentration was measured [30]. Mauna Loa is one of the so far called "Baseline Observatories" of the NOAA network, i.e., representative of the background air for a large region unaffected by local sources of pollution. In addition to Mauna Loa, observatories located at Barrow (Alaska), American Samoa, and the South Pole belong to the baseline stations. However, other ground-based stations are currently operating. Among the ground-based stations, the mentioned baseline stations and TCCON stations seem to be more reliable according to the literature [31]. The list of the worldwide ground-based stations is reported in Table A5 in the Appendix A. Tall towers are used since the 1990s to estimate the vertical CO_2 concentration gradient in continental areas and to minimize the impact of local sources and sinks [32]. Thanks to tall towers the impact of remote and local emission sources can be taken into account [33]. However, since the building of a new tall tower costs many millions of dollars [34], the realization of new towers to increase existing spatial resolution is economically infeasible. The list of the worldwide ground-based tall towers in the NOAA Earth System Research Laboratory's Global Greenhouse Gas Reference Network is reported in Table A6 in the Appendix A.

Airborne measurement has been considered in several studies as a method to collect CO_2 concentration data and to validate the satellite and ground-based measurements based on their high precision. Several means of aerial transport such as aircraft [35], helicopters [36] and balloons [37] can be utilized, and the measurement can be performed by flask sampling and/or in-situ methods. As reported by [38], the measurement of CO_2 concentration in air samples from aircraft began in 1957 at the Institute of Meteorology in Stockholm, where a specific program was performed until 1961 to take air samples at 1000 m a.s.l. Airborne measurement by means of aircraft is limited to the height of flight and the path, while the measurement by means of helicopter and balloons can provide samples at the various desired heights (vertical profile), and times, because of their ability to fly vertically; however, it will be affected by the capability of the helicopter and balloon. Concerning measurement, since it is undertaken during the flight, only one measurement for each set of spatial coordinates is allowed in case of aircraft observation. Therefore, more than one flight is required to take different measurements in a specific location. Furthermore, the sampling time interval depends on the type of observation, such as in-situ or flask sampling, and also the travel duration. In some cases, the sampling with flask is performed on the return path in order to minimize the time between measurements and the analysis, since it can affect the accuracy of the results.

Another way of collecting samples is the use of ships to cover relatively wide regions. The problem with this measurement is the necessity of a large number of ships to cover the waters in the whole world; in addition, very long times are required to cover all the world's water surfaces. However, this method is relatively cheap and affordable. The sampling time

interval and the sampling location depends on the program or the ship which is used, e.g., some sampling flasks or analyzers are installed onboard the commercial ships, and the path and times of the observation follow the defined path and time table of the journey, while the rest are installed on research ships, making it possible to plan sampling. Because of the limitation in the time intervals and sampling path of this platform, a detailed assessment of this platform will not be carried out in this study.

Due to low coverage of the airborne and ground observation, it is difficult to measure the CO_2 concentration globally; therefore, the utilization of satellite retrieval was recommended by several authors, especially for the areas with a low density of observing stations. According to Yanfang Hou et al. [39], the Scanning Imaging Absorption Spectrometer for Atmospheric Cartography (SCIAMACHY) on board ENVISAT, which was launched in 2002, is the first satellite instrument with the aim of CO_2 measurement in the lowest atmospheric layers, i.e., up to 50 km a.s.l. However, the first CO_2 concentration in the upper troposphere (less than 20 km), using satellite, was retrieved by the Advanced Earth Observing Satellite (ADEOS) in 1996, by using the Interferometric Monitor for Greenhouse Gases (IMG) [40]. Satellite observations have some advantages in comparison to other means of observation, such as high coverage, but there are several challenges such as, for example, but not limited to, the accuracy of the data, data filtration (e.g., in case of the presence of clouds), and the life span of the satellite (for example, the mission duration of ADEOS satellite was less than a year). In addition, the method which is used in satellites is different from the other methods, e.g., it is not necessary to have flask samples, which increases the pace of data observation.

The most common method for the validation of data retrieved by means of satellites is comparison with calibrated ground-based data. OCO2 and ground-based comparison was made by Wunch et al. [41], Bi et al. [42], Timofeyev et al. [43], Wu et al. [44], O'Dell et al. [45], Liang et al. [46], and Liang A. [47], considering various factors such as modes of observation, satellite data version and different bands, i.e., the channel which the OCO2 satellite measures the sunlight backscattered by the Earth's surface and atmosphere. GOSAT and ground-based observations were compared by Qin et al. [48], Dan-dan et al. [49], Velazco et al. [50], Eguchi et al. [51], Ohyama et al. [52], Rokotyan et al. [53], Yates et al. [54], Qu et al. [55], Zeng et al. [56], and Wunch et al. [57]. In many papers, several satellites were simultaneously compared with the ground-based data. Yuan et al. [58] compared the data of in-situ measurement and satellite ones, SCIAMACHY on ENVISAT, TANSO-FTS on GOSAT, and OCO2. Buchwitz et al. [59,60] during the GHG-CCI project (Climate Change Initiative (CCI)), compared TCCON data with data from SCIAMACHY/ENVISAT and TANSO/GOSAT satellites. Miao et al. [61] compared GOSAT, SCIAMACHY and AIRS with TCCON, finding that the AIRS data perform better in coverage and accuracy than the two others, in the case of the monthly mean. Avelino and Arellano [62] validated the data from AIRS, GOSAT at mid-atmosphere with ground stations. Zhang et al. [63,64] made a comparison of the data from ground stations with AIRS, SCIAMACHY, and GOSAT. Jiang et al. [65] made comparison between GOSAT, TES, AIRS, and TCCON. Reuter et al. [66] and Michael Buchwitz et al. [67] studied the difference between SCIAMACHY/ENVISAT, TANSO-FTS/GOSAT, and TCCON. Dils et al. [68] compared the TCCON data with various algorithms in different satellites and found a precision of around 2.4–2.5 ppm for almost all algorithms. Various algorithms in GOSAT were investigated by Kim et al. [69], Wunch et al. [31], Dongxu Yang et al. [70], and Lindqvist et al. [71]. These are a part of studies that have been done on difference between satellite observations and ground-based results. The available data on concentration differences of satellites and TCCON stations in these studies are illustrated in Section 3.

Several studies compared data retrieved from satellites with those from airborne measurement. However, since no measurement is possible with aircraft at altitude higher than 15 km a.s.l., stratospheric balloons are used in the range 15–35 km a.s.l. [72]. Tadic and Michalak [73] compared the data from aircraft, GOSAT and OCO2 satellites and found that the difference could be over 0.5 ppm_v between aircraft and satellites. Maddy et al. [74] made

a comparison among all available data from NOAA ESRL/GMD aircraft and AIRS during 2005, finding an agreement of around 0.5%. Chahine et al. (2005) [75] compared the annual cycle from AIRS and CONTRAIL over the western Pacific and found a good agreement with AIRS in both hemispheres. Uspensky et al. [76] applied an improved scheme for XCO_2 on AIRS data in Siberia and cloud-cleared IASI data, comparing it with the YAK-AEROSIB aircraft campaign, finding an error of 2.2 ppm_v. In another study, Kukharskii and Uspenskii [77] worked on a numerical solution for the XCO_2 data retrieved from AIRS and compared it with airborne data over the areas of boreal forests (the Novosibirsk region) and ecosystems (the region of Surgut), resulting in an error no worse than 1%. Frankenberg et al. [78] compared the data from HIPPO flights with GOSAT, TES, and AIRS concluding that over the remote Pacific Ocean the GOSAT satellite, with about 0.5 ppm accuracy, has the best performance among the 3 assessed satellites.

To investigate the difference between the measurement of CO_2 concentration by satellites and other platforms, i.e., the error of the data, the average value, and the standard deviation reported by each study was considered. To have an aggregate value, since the number of samples in each of the referenced studies is different, the average mean and the pooled standard deviation is used to combine all data sets.

The average mean of CO_2 concentration difference between satellites and other platforms is calculated as in Equation (7):

$$\mu_p = \frac{\sum_{i=1}^{N} n_i.\mu_i}{N} \quad (7)$$

where:
μ_p = The average mean difference between satellites and other platforms CO_2 concentration
μ_i = Mean difference between satellites and other platforms CO_2 concentration in each data set
n_i = Number of measurements (samples) per data set
N = Total number of measurements

The pooled standard deviation value is calculated by Equation (8) as suggested by [79]:

$$\sigma_p = \sqrt{\frac{1}{N-K}\sum_{i=1}^{N}(n_i-1).\sigma_i^2} \quad (8)$$

where:
σ_p = Pooled standard deviation
σ_i = Standard deviation in each data set
K = Number of data sets

2.3. The New Proposed Model for Atmospheric CO_2 Mass Calculation

The whole Earth surface is considered as the area of study, as the main purpose of this study is to validate a method for the calculation of the atmospheric carbon dioxide mass. The main influential factors to define the global atmospheric mass of CO_2 are (i) its concentration, (ii) total dry air mass, and (iii) air molecular weight. Considering the limited number of stations and observations in Fraser et al. [8] and the uncertainties in the listed factors, a new approach to calculate CO_2 mass is designed. The methodology is pictured in the block diagram of Figure 2. As shown, the main difference with respect to Fraser's methodology is that the new method uses higher resolution data for CO_2 concentration and is not limited to values calculated by elaborating the data coming from a few stations located around the world (block a).

Information from satellite observation was used to allocate to each cell. For this purpose, OCO2 and OCO3 satellites were considered, since they are the latest satellites launched for the carbon dioxide observation goal. OCO2 measures atmospheric carbon dioxide [80] from the Earth surface up to the satellite [81] by means of spectrometers using the reflected sunlight intensity from CO_2 in a column of air instead of direct measurement. Wavelength bands which are measured by OCO2 are 0.765 μm, related to oxygen, and two

CO_2 bands at 1.61 µm and 2.06 µm [82]. Diffraction grating is used to separate the reflected light energy into a spectrum of multiple component colours [83].

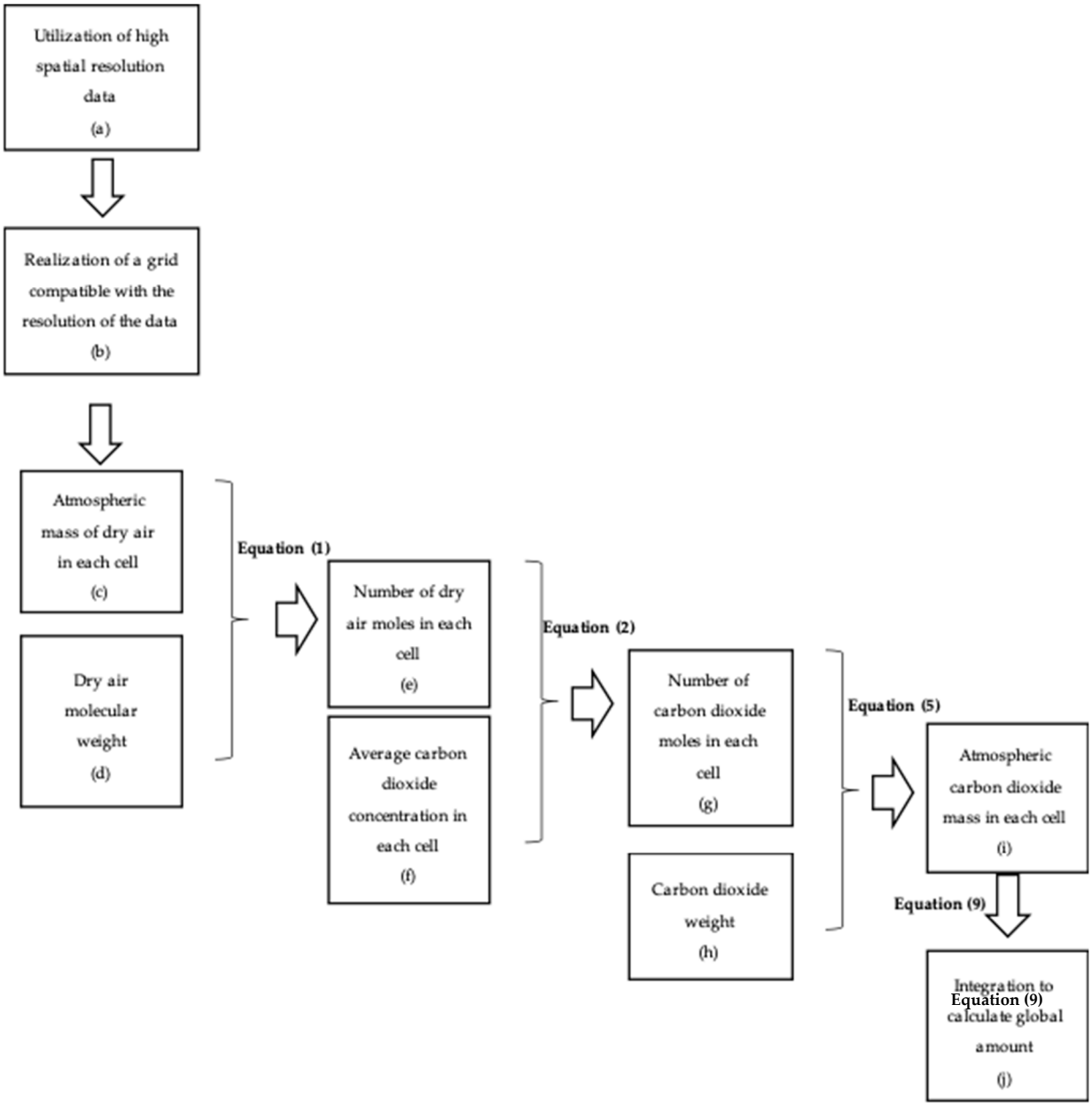

Figure 2. Building blocks for the proposed methodology to reach a higher accuracy of the results for global atmospheric carbon content. Letters (**a**–**j**) are used to label the blocks in order to simplify mentioning the steps in the text.

OCO2 was launched on 2 July 2014, and it orbits at 705 km elevation; it captures approximately 1 million soundings each day, of which around 10% are aerosols/cloud free which could be used to measure XCO_2 [81]. Temporal resolution of OCO2 is 16 days and its spatial resolution is 2.25 km × 1.29 km [80].

Considering the satellite daily orbit coverage, it was decided to use 4-day data as the complete surface coverage. As shown in Figure A3, in the Appendix A, for OCO2, the satellite takes almost four days to cover the entire Earth surface. Furthermore, it is assumed that the change of the global CO_2 atmospheric mass is negligible in four days. Therefore, the 4-day observation was chosen as a representative to calculate the CO_2 global atmospheric mass.

Bias-corrected data from both satellites were assessed to check the applicability of the data. OCO2 and OCO3 satellites' bias-corrected files, version 9r, were taken from the NASA website [80]. The data were in the netCDF format. R programming language was used to extract the desired data, namely, the longitude, latitude, quality flag, XCO_2 (that is the column average carbon dioxide concentration in each cell), total water vapor column, and surface pressure. In particular, the quality flag defines if the data are acceptable or not. Data with a quality flag equal to 1 was not accepted in accordance with OCO2 and OCO3 documentation [84] and not considered in the following elaborations. Based on a preliminary analysis, it was decided to use only data from OCO2. In fact, OCO3 was characterized by a low number of observations that passed the quality flag filtration, around 40,000 observations in average for each day of 4-day observation. Furthermore, OCO3 data were available only since August 2019, and data were missing for several days.

A computational grid compatible with the data's resolution was designed to divide the Earth's surface into cells (block b). Since the Earth's surface is 514,720,000 km^2 and each cell has an area of 2.90 km^2 (=2.25 km × 1.29 km), that is the spatial resolution of the satellites used in the calculation; approximately 177,500,000 cells (514,720,000/2.90) are considered.

The following steps (from block c to block i) are essentially the same as Fraser's methodology but they are applied to each cell. Codes were written in MATLAB for the elaboration of the data while the available "curve fitting" was applied to do regression. It should be noted that to calculate the atmospheric mass of dry air in each cell (block c), data about the total surface pressure and the column of water vapor was taken from the NASA website [80]. Through Dalton's Law, the dry air pressure in each cell was calculated. Thus, the dry air mass, which can be used in Equation (1), can be calculated, considering the cell area and gravity.

The final step is the summation of the cell values to calculate the global CO_2 atmospheric mass by Equation (9):

$$CO_{2,gac} = \frac{\sum_{i=1}^{N_c}\left(\frac{CO_{2,cac,i}}{2.25\times1.29}\right)}{N_c} \times S_{earth} \quad (9)$$

where:
$CO_{2,cac,I}$ = CO_2 mass in the i-th cell
N_c = number of cells
S_{earth} = Earth surface, i.e., 510.1 × 10^6 km^2

To validate the proposed model, Fraser's model [8] was applied. Assuming the CO_2 concentration data from NOAA, the global CO_2 atmospheric mass was calculated for the period from 1980 to 2021. However, since the elaboration of the model is time-consuming, the global CO_2 atmospheric mass from OCO2 was calculated for 2019 and 2020.

3. Results and Discussion

3.1. Validation of the Simplified Fraser's Method for the Calculation of CO_2 Atmospheric Mass

The authors calculated the global amount of CO_2 mass by assuming an average CO_2 atmospheric concentration of 337.04 ppm_v, based on a two-dimensional global atmospheric CO_2 transport model calibrated through the data from 21 stations [85]. To calibrate the model, the authors calculated the difference between the CO_2 annual mean concentration in each station, with the South Pole station taken as reference.

Based on Equation (6), and the average global concentration calculated by Fraser et al., the amount of global CO_2 mass was calculated as shown in Equation (10). More than 2.6 × 10^{15} kg of CO_2 resulted by the application of the methodology proposed by the authors

$$CO_{2,gac} = 337.04 \times \frac{5.12\times10^{18}}{0.02897} \times 10^{-6} \times 44.01 \times 10^{-3} = 2.62 \times 10^{15} kg \quad (10)$$

The authors calculated also the global carbon mass equal to 7.15×10^{14} kg, simply by the substitution of the CO_2 molecular weight with carbon molecular weight in Equation (6).

According to Equation (6), the average global carbon dioxide concentration, the global atmospheric mass of dry air, and dry air mean molecular weight affect CO_2 mass estimation. The authors declared a probable uncertainty of 0.5 to 1% relating to carbon mass calculation divided as:

- 0.4–0.9% related to CO_2 concentration. Only 21 stations were considered to design and calibrate the model as representative of the entire world. Furthermore, no stations were located in Europe, Asia, Africa, and South America, resulting in unbalanced earth surface coverage. In addition, the number of observations in which the annual mean CO_2 concentration is calculated is not provided in Fraser's study. Therefore, it is not possible to evaluate if the reported values cover all diurnal, daily, weekly, monthly, and seasonal changes or not.
- 0.1% for the air global atmospheric mass and the air mean molecular weight. Concerning the global atmospheric mass of dry air, a value equal to 5.12×10^{18} kg was used in the model. However, in 1994 a more accurate estimation of around 5.132×10^{18} kg was given by Trenberth and Guillemot [86], while, in 2005, Trenberth and Smith [87] estimated the dry air mass as $5.1352 \pm 0.0003 \times 10^{18}$ kg. With respect to Fraser's model, an error equal to 0.29% results. Concerning the dry air average molecular weight, the effect of boundary conditions such as temperature and humidity is not taken into account.
- By comparing the reported global atmospheric carbon dioxide mass in Fraser's study and the result achieved by applying the information from this study in the Equation (6), it can be assumed that the procedure used in Fraser's study is the same as Figure 1. Considering the complexity of Fraser's method, the paper shows how it is possible to work on a simpler methodology with similar or even higher accuracy.

3.2. Assessment and Comparison of Existing Platforms

Existing platforms are compared through the definition of suitable Key Performance Indicators (KPI), as shown in Table 1. In this table, "ground-based stations", "aircraft, helicopter and balloon", "satellites" and "ships" are compared based on the available literature at the state of the art, including measurement accuracy, precision, coverage, and time. Based on the measurements described in the literature, as shown in Table 1, the accuracy of the data is almost the same, less than 0.5 ppm, except for ships where different instruments were used by researchers resulting in a wide interval of accuracy.

Almost all platforms could have high accuracy and precision, and the distinctive indices which make a difference between the platforms seem to be the coverage and the time scale required for observation. As can be seen, for the global observation the choice could be use of satellite data. However, it is possible to use other platforms and global atmospheric transport models to estimate the global atmospheric carbon dioxide concentration.

The temporal resolution of satellites provided in this table is related to the satellites which are operating, and the data available. The temporal resolution of the satellites is higher compared to the other platforms if global coverage is desired.

Since the variation in the carbon dioxide concentration related to the surface sinks and sources are typically less than 1 ppm, and seasonal and annual XCO_2 variation are small in comparison to the mean atmospheric concentration, thus, 1–2 ppm precision is needed for satellite retrievals [88].

Table 1. KPI table of the means of observations.

Means of Observation	Accuracy [a]	Precision	Cost [b]	Coverage	Time Scale
Ground-based stations	Could be ±0.5 ppm	Better than 0.25% for TCCON	low-high [c]	local-regional [d]	Sampling and Analysing duration
Aircraft, Helicopters and Balloons	Could be less than ±0.25 ppm (±0.1, ±0.05 ppm are also obtained)	Could be ±0.1 ppm	low-high [c]	regional	Flight and Analysing duration [e]
Ships	N/A [a]	Could be better than 0.6%	low	regional	Travel duration + Analysing duration [c]
Satellites	−0.08 ppm regarding TCCON according to the calculations	Less than 2 ppm is needed	high	global	OCO2 & OCO3-16 days GOSAT-3 days

Notes: [a] It depends on the utilized instrument. [b] The satellite cost is assumed to be the comparison base. [c] In case of network it is expensive. [d] Regarding the elevation of the sampling vessel and filtering approach, this can be representative of local or regional. In case of combination of the stations in a network with models it is possible to have the global coverage. [e] It can be only sampling and analyzing duration if the analyzing instruments are installed in the means of observation.

3.3. Comparison of CO_2 Concentration Measured by Satellites with TCCON

Figure A2 illustrates the comparison of satellite observations and TCCON stations based on the data provided in Table A4. Since satellites' observations are compared in Table 1 to show the accuracy and reliability, various satellites are compared with TCCON in this figure. By using the mentioned formula, and the data available in Table A4 in the Appendix A, it is possible to calculate the average mean and pooled standard deviation of the datasets for which the number of observations is provided in the context of the papers. As can be seen in this figure, the mean difference range is between −2 and 2 ppm and mean ± standard deviation ranges between −5 and 4 ppm. According to Equations (7) and (8), the mean average of the comparison between satellites and TCCON is −0.08 ppm and the pooled standard deviation is ±1.66 ppm.

3.4. Global Atmospheric CO_2 Mass Calculation

The application of Fraser's methodology to the NOAA data gives the results shown in Figure A4 in the Appendix A. As shown, a continuously increasing trend occurs in the period. The atmospheric CO_2 mass increased up to 3.22×10^{15} kg in 2021, corresponding to a yearly increase of around 1.44×10^{10} tons per year between 1980 and 2021.

The proposed model was applied to OCO2 data, resulting in Figure 3 for the period 1 January 2019 to 31 November 2020. The yellow line is the global CO_2 atmospheric mass calculated using the data of the satellite based on the methodology proposed in this paper. The blue line is a 12th polynomial regression curve for the global atmospheric CO_2 mass calculated by the satellite ($R^2 = 0.71$). The dark line is the curve designed from the data obtained by NOAA measurements applying Fraser's methodology, ($R^2 = 0.86$). Since the polyline regression with high degrees results in huge anomalies in the boundary of data the last part is neglected, and the assumed trend is provided, which is shown in the dashed red line. The available CO_2 mean concentrations reported in NOAA database are weekly and monthly, of which the monthly one is used in this study. It can be seen that there is less variation in the curve related to NOAA database which goes back to the difference between the time frames.

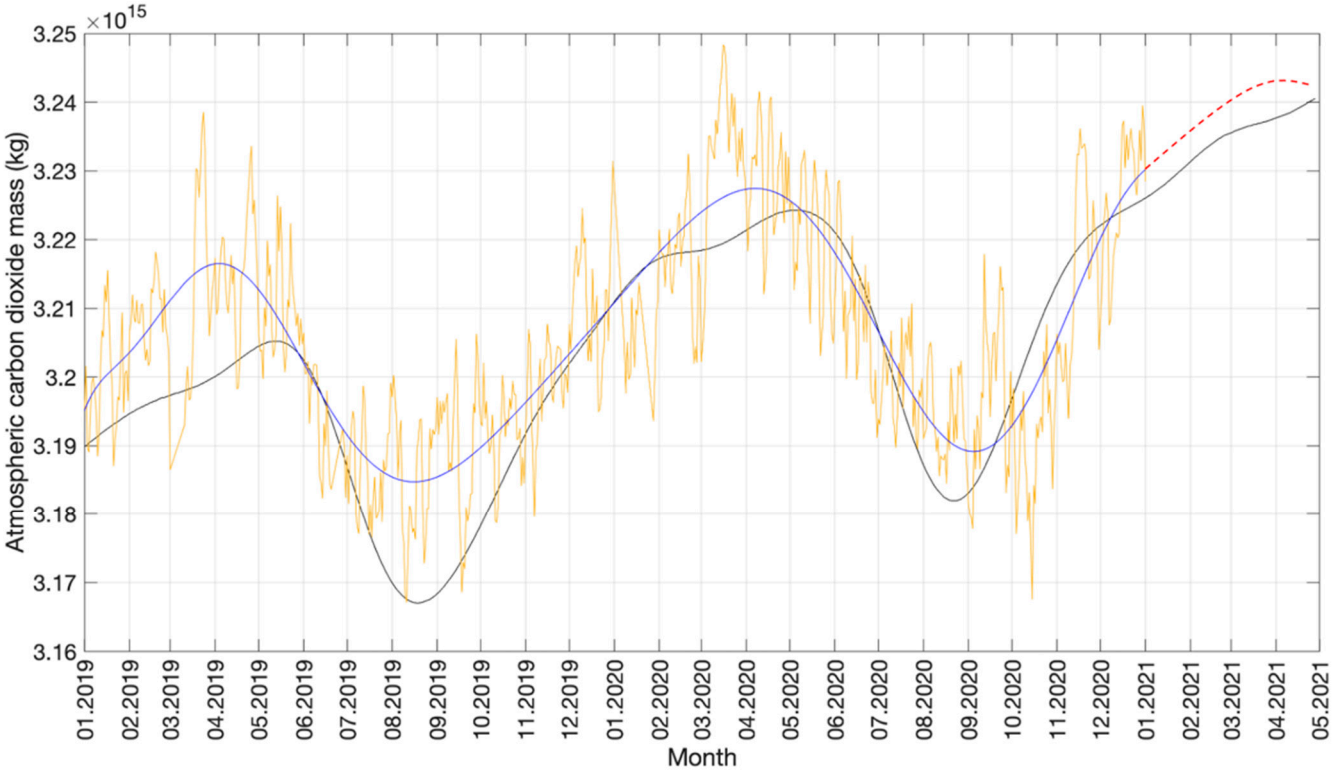

Figure 3. OCO2 global 4-day carbon dioxide mass estimation in the period 2019–2021. The orange is 4-day global atmospheric carbon dioxide mass estimation, the black curve is related to NOAA data, and the blue is the fitting curve. The red dashed line is the prediction of global carbon dioxide mass since the data was not available for OCO2.

As shown by the trend, the CO_2 mass reaches its peak approximately between March and May, while the minimum occurs in the period between August and November. An upward seasonal trend of global atmospheric CO_2 mass appears. The seasonal changes are probably due to various natural and anthropogenic parameters, which are different between the NH and SH. During spring and the beginning of summer in the NH, global atmospheric CO_2 mass reaches its annual maximum. At the same time, the minimum happens at the end of summer and during the NH's autumn.

Figure 3 shows the 2019–2021 period; the same cyclic trend appears in the global mass calculation using Fraser's method and the proposed methodology. In this figure, a good agreement appears between the two methodologies. In fact, a slight difference exists between Fraser's methodology using the NOAA dataset and the proposed methodology. By comparing the fitting curve and black curve it can be seen that the results are almost the same except for extremums, and May-July is the period with the best consistency of results.

Table 2 summarizes the differences during the period 2019–2020. As shown, a slightly greater amount of CO_2 was calculated with the proposed methodology. A maximum difference of 1.25% was calculated for August 2019, while for 2020 the maximum difference was around 0.3%. Finally, an average difference of 0.15% was calculated for the entire investigating period. These differences could be due to the assumptions made in Fraser's method, a lower number of observations and the amount of total water vapor column and surface pressure in each cell to calculate dry air moles for each cell instead of the whole Earth. Since both methods give estimations of atmospheric carbon dioxide mass it is not possible to determine which method is more accurate. However, given the use of a wider data set and the process of considering parameters separately for each observation column in the methodology proposed in this study, it seems that our proposed approach is more accurate.

Table 2. Comparison of the global atmospheric carbon dioxide mass using NOAA data and OCO2 data, 2019–2020.

	NOAA CO2 Mass Results	OCO2 Data CO2 Mass Results
Average value (kg)	3.201 × 1015	3.206 × 1015
Maximum value (kg)	3.226 × 1015	3.248 × 1015
Minimum value (kg)	3.167 × 1015	3.167 × 1015
Maximum difference ((OCO2–NOAA)/NOAA)	1.23%	
Average difference	0.15%	

Based on these results, the validation of the methodology is assumed successful. One of the most feature of the proposed methodology in this study is its spatio-temporal flexibility; it is possible to estimate the global atmospheric carbon dioxide mass with acceptable accuracy for desired dates; in addition, since the amount of CO_2 mass is calculated for each cell during the procedure, it is possible to define the CO_2 mass and its variation in desired locations. A similar approach for CO_2 column averaged concentrations was proposed by [89] to investigate the trend over the Indian region. For this purpose, data from SCHIAMACHY and GOSAT were used. Based on the proposed approach, the authors theorize the potential links between seasonal concentrations trends and anthropogeneous behaviour. Similarly, [90] investigated the spatial distribution of the annual average atmospheric CO_2 for the state of Mato Grosso (Brazil) using data from OCO2 lite version (V8r). However, both studies do not calculate the CO_2 mass amount in the atmosphere as done by the proposed model. Therefore, they do not allow determination of the nominal capacity of the CO_2 carbon capture, storage and utilization plants as required for national targets in terms of climate mitigation. In addition, the flexibility provided by the methodology could be useful for control of the anthropogenic activities and to monitor performance of the mitigation and adaptation strategies. However, other aspects such as alteration in carbon sinks should be taken into account since the reported CO_2 mass is the balance between carbon source and carbon sink.

4. Conclusions

One of the most important GHGs is carbon dioxide due to its long-lasting presence in the atmosphere and negative impact on climate change. Therefore, the accurate estimation of the atmospheric CO_2 mass is crucial to propose mitigation measures and assess their impact. However, the method of calculation has not changed since 1983, even though new measuring platforms, i.e., the satellites, and more data are available. In particular, satellite observation is more reliable for global scale estimation, considering its spatial and temporal resolution. The mean average of the comparison between satellites and TCCON is -0.08 ppm, and the pooled standard deviation is ± 1.66 ppm. Among the satellites launched for the purpose of CO_2 measurement, the most recently launched satellites, OCO2 and OCO3, were considered to assess their applicability for the new methodology. Due to a low fraction of acceptable observations, after quality flag filtration, and missing days in the OCO3 observation, it was decided to use data from OCO2.

The proposed methodology ensures high resolution to estimate the global atmospheric carbon dioxide using a wide range of observations and better results with respect to the ones that can be obtained by Fraser's methodology as currently applied. The maximum and average difference between the proposed method and the results of Fraser's method using NASA data were 1.23% and 0.15%, respectively. Although very accurate models based on observations and chemical transport are available in the literature, the proposed approach could be applied in those cases where computing power or atmospheric data are limited.

Since the proposed methodology divides the Earth into cells according to the satellite spatial resolution, the local and global atmospheric CO_2 mass distribution can be assessed. The main issue in this study is related to the availability of data from satellites which might

be addressed by combination of satellites or using proper algorithms to reproduce missed data. The result of this study could be helpful in decision-making for the installation of systems for carbon capture and finding the most critical locations in the world to make a plan for climate change mitigation and adaptation. The application of the methodology for such purposes will be shown in a future paper by the authors.

Author Contributions: Conceptualization, M.P., A.A., A.G. and C.S.; Data curation, A.A.; Formal analysis, A.A.; Investigation, A.A.; Methodology, A.A. and A.G.; Project administration, A.G.; Software, A.A.; Supervision, M.P. and A.G.; Validation, M.P., A.G. and C.S.; Visualization, M.P., A.A. and C.S.; Writing—original draft, A.A.; Writing—review and editing, M.P., A.G. and C.S. All authors have read and agreed to the published version of the manuscript.

Funding: This research received no external funding.

Institutional Review Board Statement: Not applicable.

Informed Consent Statement: Not applicable.

Data Availability Statement: The data presented in this study are openly available in www.esrl.noaa.gov and https://disc.gsfc.nasa.gov (accessed on 7 August 2021).

Acknowledgments: The used data were produced by the OCO-2 project at the Jet Propulsion Laboratory, California Institute of Technology, and obtained from the OCO-2 data archive maintained at the NASA Goddard Earth Science Data and Information Services Center.

Conflicts of Interest: The authors declare no conflict of interest.

Appendix A

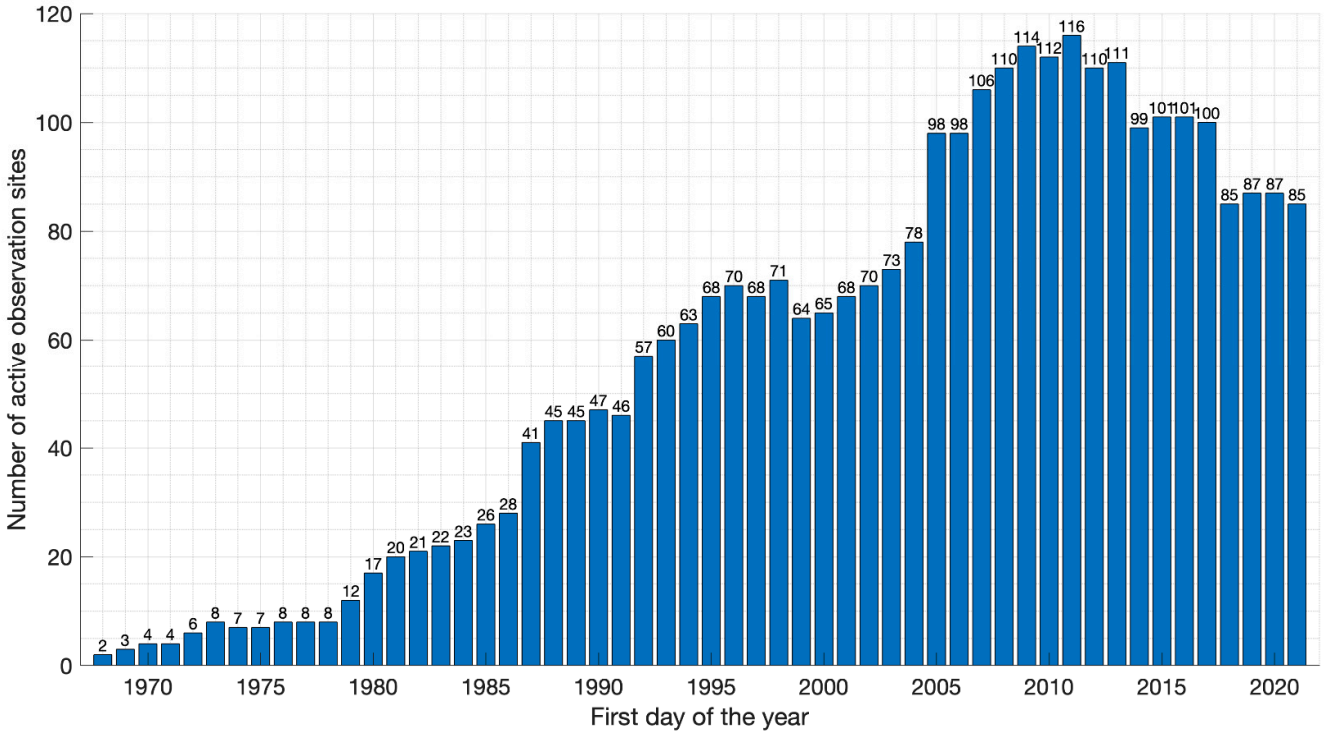

Figure A1. The number of active observation sites at the beginning of each year. Data elaborated from the information reported in Table A3 in the Appendix A.

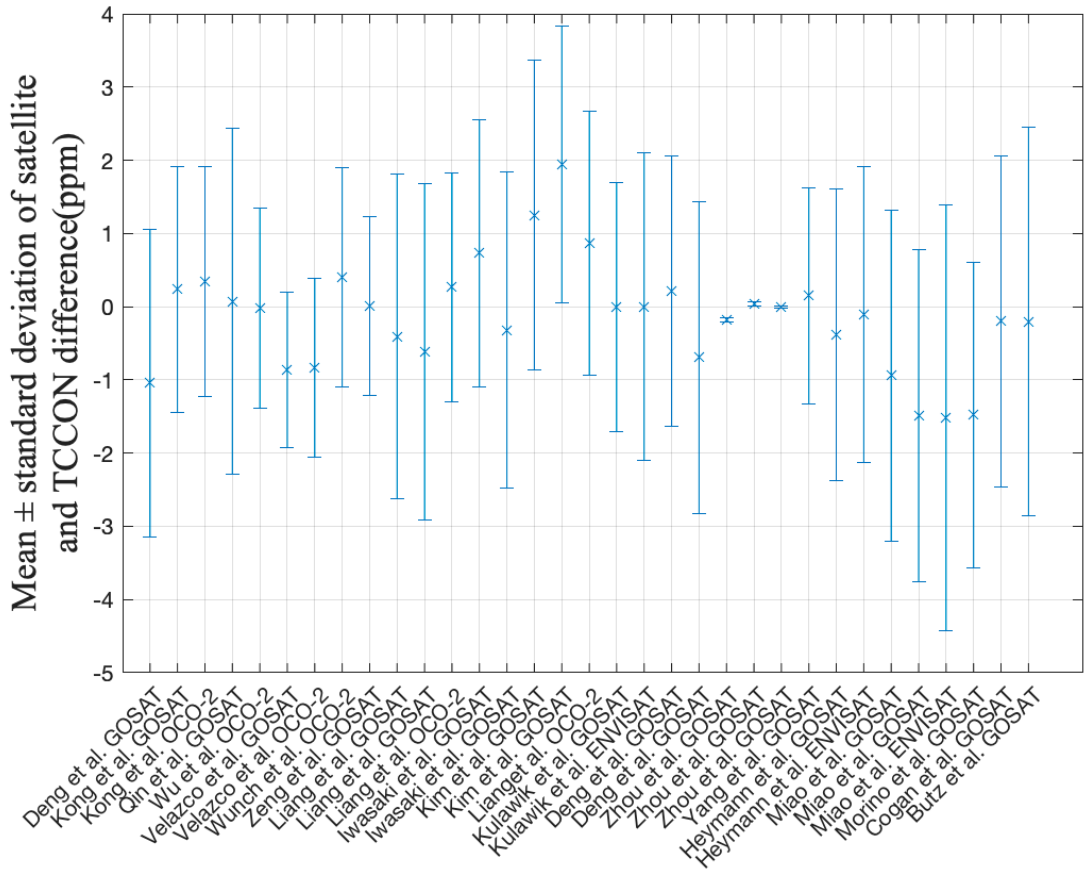

Figure A2. Comparison of satellite observations and TCCON stations (References detail are provided in the Table A4 in the Appendix A.). The different studies are labelled based on references.

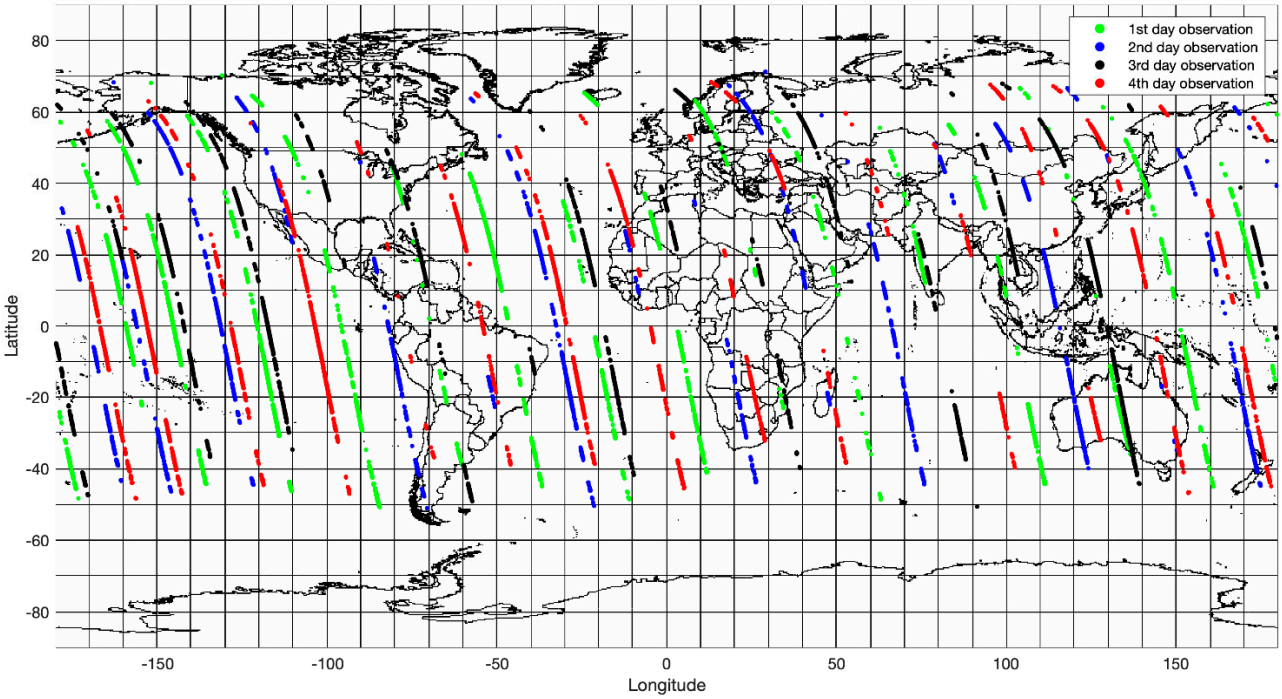

Figure A3. OCO2 4-day observation, 22.04.2019–25.04.2019.

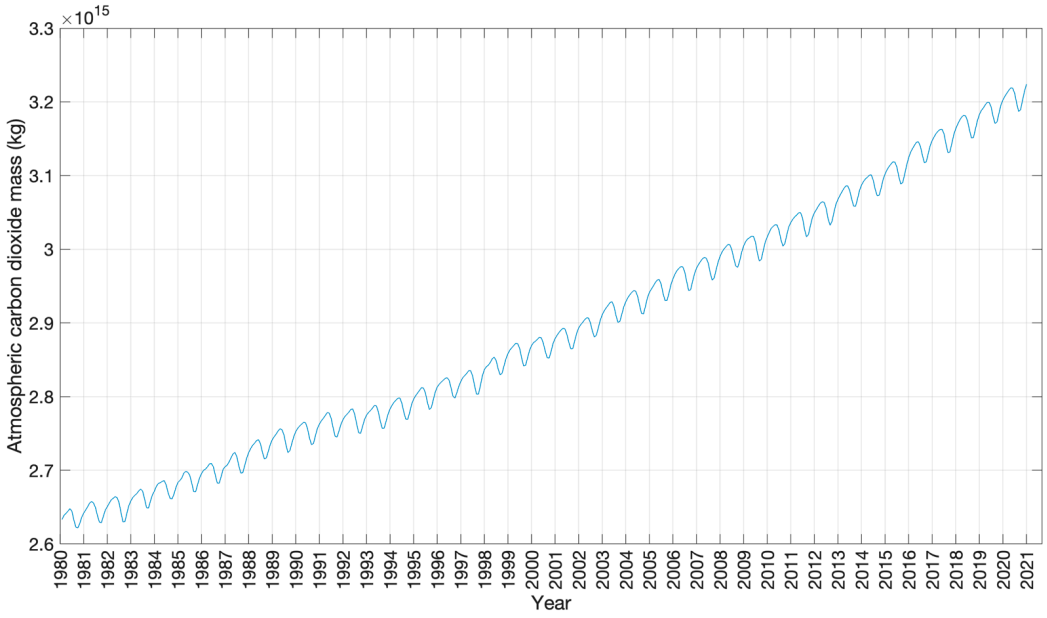

Figure A4. Global atmospheric carbon dioxide mass 1980–2021.

Table A1. Stations data adapted with permission from Fraser et al. [8] for 1980. Copyright 1983 by the American Geophysical Union.flask is sampling and in-situ is the measurement performed in the site.

No.	Name	Symbol	Latitude	Longitude	Flask (F) or In Situ (I)	Concentration [a], [ppmv]
1	Bass Strait	BAS	−40°	150°	F	336.7
2	Cape Grim	CGO	−41°	145°	F I	335.5 336.5
3	Macquarie Island	MAQ	−54°	159°	F	336.9
4	Mawson	MAW	−68°	61°	F	335.5
5	Amsterdam Island	AMS	−38°	78°	F	337.4
6	Ascension Island	ASC	−8°	−14°	F	338.5
7	Azores	AZO	38°	−27°	F	340.2
8	Barrow	BRW	71°	−157°	F I	340.7 339.7
9	Cape Kumukahi	KUM	20°	−145°	F	340
10	Cold Bay	CBA	55°	−163°	F	340.2
11	Guam	GUA	13°	145°	F	340.9
12	Key Biscayne	KEY	26°	−80°	F	340.7
13	Mauna Loa	MLO	20°	−156°	F I	341.2 338.1
14	Mould Bay	MOB	76°	−119°	F	340.5
15	Niwot Ridge	NWR	40°	−105°	F	340.4
16	Point Six Mount	PSM	47°	−114°	F	341
17	Samoa	SMO	−14°	−170°	F I	337.9 337.9
18	Seychelles	SEY	−5°	55°	F	338.6
19	South Pole	SPO	−90°	0	F I F	336.1 335.9 337
20	St. Croix	AVI	18°	−65°	F	339.9
21	Fanning Island	FAN	4°	−159°	F	339.1

Note: [a] the concentration was referred to 1980.

Table A2. Effective parameters on carbon dioxide concentration.

No.	Author	Year of Publishment	CO2 Sources [1]	Meteorological Parameters [2]	Atmospheric Boundary Layer Height Cycle [3]	Vegetation and Climate	Population, GDP and Employment	Surface Complexity and Albedo	Soil Respiration and Terrestrial Ecosystem	Sampling Time [4]	Observation Characteristics and Height	Wildfire	Phytoplankton and Ocean	Aerosols, Clouds and Fog
1	M. N. Patil et al. [91]	2020												✓
2	Yanfen Li et al. [92]	2019												✓
3	Zhaleh Siabi et al. [93]	2019		✓		✓								
4	Ivakhov V. et al. [94]	2019										✓		
5	Swma Jamalalden Al-jaf, Osama Tareq Al-Taai [95]	2019				✓								
6	Irène Xueref-Remy et al. [96]	2018	✓	✓	✓									
7	Mahesh Patakothi et al. [97]	2018		✓										
8	Shuai Yin et al. [98]	2018		✓		✓							✓	
9	Michael Buchwitz et al. [67]	2018		✓										
10	Nian Bie et al. [99]	2018						✓						✓
11	Ge Han et al. [100]	2018									✓			
12	Xun Jiang et al. [101]	2017		✓										
13	Seyed Mohsen Mousavi et al. [102]	2017				✓								
14	Samereh Falahatkar et al. [103]	2017		✓		✓								
15	LEI Li Ping et al. [104]	2017	✓											
16	Debra Wunch et al. [41]	2017						✓						✓
17	Jacob K. Hedelius et al. [105]	2017	✓	✓	✓									
18	Koorosh Esteki et al. [106]	2017	✓	✓										
19	Chen Pan et al. [107]	2016	✓			✓								
20	Thomas E. Taylor et al. [108]	2016												✓
21	Yeonjin Jung et al. [109]	2016												✓
22	Hernández-Paniagua et al. [110]	2015		✓										
23	Min Liu et al. [111]	2015	✓											
24	LIU Xiao-Man et al. [112]	2015	✓			✓								
25	H. Ohyama et al. [52]	2015												✓
26	Loretta Gratani and Laura Varone [113]	2014	✓			✓								

Table A2. *Cont.*

No.	Author	Year of Publishment	CO2 Sources [1]	Meteorological Parameters [2]	Atmospheric Boundary Layer Height Cycle [3]	Vegetation and Climate	Population, GDP and Employment	Surface Complexity and Albedo	Soil Respiration and Terrestrial Ecosystem	Sampling Time [4]	Observation Characteristics and Height	Wildfire	Phytoplankton and Ocean	Aerosols, Clouds and Fog
27	Moon-Soo Park et al. [114]	2014		✓	✓			✓						
28	S. X. Fang et al. [115]	2014		✓										
29	Qin XC et al. [116]	2014									✓			
30	Yanli Li et al. [117]	2014	✓	✓					✓					
31	M. Górka and D. Lewicka-Szczebak [118]	2013	✓						✓					
32	Li Yan-li et al. [119]	2013		✓										
33	Christian Büns and Wilhelm Kuttler [120]	2012	✓	✓										
34	Jiabing Wu et al. [121]	2012		✓		✓								
35	Ma Ángeles García et al. [122]	2012		✓										
36	Yanfang H. [123]	2012	✓			✓			✓					
37	Andrew Rice and Gregory Bostrom [124]	2011	✓		✓	✓								
38	Ramamurthy P. and Pardyjak ER. [125]	2011				✓								
39	Irène Xueref-Remy et al. [126]	2011				✓								
40	Ke Wang et al. [127]	2011	✓	✓					✓					
41	Nawo Eguchi et al. [51]	2011	✓			✓							✓	✓
42	Y. Yoshida et al. [128]	2011						✓			✓			✓
43	C. Sirignano et al. [129]	2010								✓				
44	Ch. Gurk et al. [130]	2008				✓								
45	George L. H. Ziska et al. [131]	2007	✓				✓							
46	I. Aben et al. [132]	2007												✓
47	Yang Y. et al. [133]	2006		✓										✓
48	Loretta Gratani and Laura Varone [134]	2005	✓	✓										
49	Hassan A. Nasrallah et al. [135]	2003	✓	✓		✓								
50	P. Chamard et al. [136]	2003		✓										
51	Yuesi et al. [137]	2002								✓				
52	Elizabeth A. Wentz et al. [138]	2002	✓				✓							

Table A2. *Cont.*

No.	Author	Year of Publishment	CO2 Sources [1]	Meteorological Parameters [2]	Atmospheric Boundary Layer Height Cycle [3]	Vegetation and Climate	Population, GDP and Employment	Surface Complexity and Albedo	Soil Respiration and Terrestrial Ecosystem	Sampling Time [4]	Observation Characteristics and Height	Wildfire	Phytoplankton and Ocean	Aerosols, Clouds and Fog
53	Richard J. Engelen et al. [139]	2001												✓
54	T. J. Conway et al. [140]	1988			✓									

[1]. anthropogenic sources such as urban sources (heating, and traffic), industry; [2]. wind speed and direction, precipitation, humidity, temperature, pressure, solar radiation and drought, La Niña and El Niño events; [3]. depends on the elevation of the location; [4]. in the afternoon for well mixing of the air.

Table A3. Sites that are currently included in the global gas reference network [141].

Site	Name	Location	First Carbon Dioxide Dataset	Status Carbon Dioxide Dataset	Air Sample Collection Method
1	Airborne Aerosol Observatory	Bondville (USA)	07.06.2006	Terminated 18.09.2009	Airborne Flasks *
2	Arembepe, Bahia	Brazil	27.10.2006	Terminated 13.01.2010	Surface Flasks *
3	Alaska Coast Guard	United States	30.04.2009	Terminated 21.10.2017	Airborne Flasks *
4	Alert, Nunavut	Canada	10.06.1985	ongoing	Surface Flasks
5	Amsterdam Island	France	05.01.1979	Terminated 07.12.1990	Surface Flasks *
6	Argyle, Maine	United States	18.09.2003 22.11.2008	Terminated 29.12.2008 ongoing	In Situ Tall Tower Surface Flasks
7	Anmyeon-do	Republic of Korea	03.12.2013	ongoing	Surface Flasks
8	Ascension Island	United Kingdom	27.08.1979	ongoing	Surface Flasks
9	Assekrem	Algeria	12.09.1995	ongoing	Surface Flasks
10	St. Croix, Virgin Islands	United States	16.02.1979	Terminated 29.08.1990	Surface Flasks *
11	Terceira Island, Azores	Portugal	26.12.1979	ongoing	Surface Flasks
12	Baltic Sea	Poland	31.08.1992	Terminate 22.06.2011	Surface Flasks *

Table A3. *Cont.*

Site	Name	Location	First Carbon Dioxide Dataset	Status Carbon Dioxide Dataset	Air Sample Collection Method
13	Boulder Atmospheric Observatory, Colorado	United States	16.08.2007	Terminated 06.07.2016	In Situ Tall Tower * Airborne Flasks * Surface Flasks *
14	Bradgate, Iowa	United States	13.09.2004	Terminated 18.11.2005	Airborne Flasks *
15	Baring Head Station	New Zealand	14.10.1999	ongoing	Surface Flasks
16	Bukit Kototabang	Indonesia	08.01.2004	ongoing	Surface Flasks
17	St. Davids Head, Bermuda	United Kingdom	13.02.1989	Terminated 25.01.2010	Surface Flasks *
18	Tudor Hill, Bermuda	United Kingdom	11.05.1989	ongoing	Surface Flasks
19	Beaver Crossing, Nebraska	United States	15.09.2004	Terminated 11.05.2011	Airborne Flasks *
20	Barrow Atmospheric Baseline Observatory	United States	25.04.1971	ongoing	In Situ Observatory Surface Flasks
21	Black Sea, Constanta	Romania	11.10.1994	Terminated 26.12.2011	Surface Flasks *
22	Brentwood, Maryland	United States	25.09.2018	ongoing	Surface Flasks
23	Briggsdale, Colorado	United States	09.11.1992	ongoing	Airborne Flasks
24	Cold Bay, Alaska	United States	21.08.1978	ongoing	Surface Flasks
25	Cape Grim, Tasmania	Australia	19.04.1984	ongoing	Surface Flasks
26	Christmas Island	Republic of Kiribati	08.03.1984	ongoing	Surface Flasks
27	Cherskii	Russia	Not for CO2	Not for CO2	Surface In Situ *
28	Centro de Investigacion de la Baja Atmosfera (CIBA)	Spain	05.05.2009	ongoing	Surface Flasks
29	Offshore Cape May, New Jersey	United States	17.08.2005	ongoing	Airborne Flasks
30	Cape Meares, Oregon	United States	10.03.1982	Terminate 18.03.1998	Surface Flasks *
31	Cosmos	Peru	23.06.1979	Terminate 28.05.1985	Surface Flasks *
32	Cape Point	South Africa	11.02.2010	ongoing	Surface Flasks
33	Carbon in Arctic Reservoirs Vulnerability Experiment (CARVE)	United States	29.06.2012	ongoing	In Situ Tall Tower Airborn Flasks * Surface Flasks

Table A3. *Cont.*

Site	Name	Location	First Carbon Dioxide Dataset	Status Carbon Dioxide Dataset	Air Sample Collection Method
34	Crozet Island	France	03.03.1991	ongoing	Surface Flasks
35	Dahlen, North Dakota	United States	21.09.2004	Terminated 15.11.2016	Airborne Flasks
36	Drake Passage	N/A	07.04.2003	ongoing	Surface Flasks
37	Dongsha Island	Taiwan	05.03.2010	ongoing	Surface Flasks
38	Easter Island	Chile	04.01.1994	ongoing	Surface Flasks
39	Estevan Point, British Columbia	Canada	22.11.2002	ongoing	Airborne Flasks
40	East Trout Lake, Saskatchewan	Canada	15.10.2005	Terminated 22.03.2020	Airborne Flasks *
41	Falkland Islands	United Kingdom	31.10.1980	Terminated 04.02.1982	Surface Flasks *
42	Fortaleza	Brazil	09.12.2000	Terminated 25.03.2003	Airborne Flasks *
43	Fairchild, Wisconsin	United States	20.09.2004	Terminated 18.11.2005	Airborne Flasks *
44	Mariana Islands	Guam	24.09.1978	ongoing	Surface Flasks
45	Dwejra Point, Gozo	Malta	11.10.1993	Terminated 12.02.1999	Surface Flasks *
46	Molokai Island, Hawaii	United States	31.05.1999	Terminated 22.04.2008	Airborne Flasks *
47	Halley Station, Antarctica	United Kingdom	17.01.1983	ongoing	Surface Flasks
48	Harvard Forest, Massachusetts	United States	02.03.2016	ongoing	Airborne Flasks * Surface Flasks
49	Homer, Illinois	United States	16.09.2004	ongoing	Airborne Flasks
50	Hohenpeissenberg	Germany	06.04.2006	ongoing	Surface Flasks
51	Humboldt State University	United States	17.05.2008	Terminated 31.05.2017	Surface Flasks *
52	Hegyhatsal	Hungary	02.03.1993	ongoing	Surface Flasks
53	Storhofdi, Vestmannaeyjar	Iceland	02.10.1992	ongoing	Surface Flasks
54	INFLUX (Indianapolis Flux Experiment)	United States	09.10.2010	ongoing	Airborne Flasks * Surface Flasks
55	Grifton, North Carolina	United States	30.07.1992	Terminated 09.06.1999	In Situ Tall Tower * Surface Flasks *
56	Izana, Tenerife, Canary Islands	Spain	16.11.1991	ongoing	Surface Flasks

Table A3. *Cont.*

Site	Name	Location	First Carbon Dioxide Dataset	Status Carbon Dioxide Dataset	Air Sample Collection Method
57	Kaashidhoo	Republic of Maldives	02.03.1998	Terminated 15.07.1999	Surface Flasks *
58	Key Biscayne, Florida	United States	13.12.1972	ongoing	Surface Flasks
59	Kitt Peak, Arizona	United States	20.12.1982	Terminated 31.10.1989	Surface Flasks *
60	Cape Kumukahi, Hawaii	United States	12.01.1971	ongoing	Surface Flasks
61	Sary Taukum	Kazakhstan	12.10.1997	Terminated 15.08.2009	Surface Flasks *
62	Plateau Assy	Kazakhstan	15.10.1997	Terminated 05.08.2009	Surface Flasks *
63	LA Megacities	United States	05.11.2014	Terminated 08.10.2017	Surface Flasks *
64	Park Falls, Wisconsin	United States	29.11.1994 05.10.2006	ongoing ongoing	In Situ Tall Tower Airborne Flasks Surface Flasks
65	Lewisburg, Pennsylvania	United States	28.02.2013	ongoing	Surface Flasks
66	Lac La Biche, Alberta	Canada	30.01.2008	Terminated 26.02.2013	Surface Flasks *
67	Lulin	Taiwan	01.08.2006	ongoing	Surface Flasks
68	Lampedusa	Italy	12.10.2006	ongoing	Surface Flasks
69	Mould Bay, Northwest Territories	Canada	13.04.1980	Terminated 26.05.1997	Surface Flasks *
70	Mt. Bachelor Observatory	United States	14.10.2011 03.05.2012	ongoingongoing	Surface Flasks Surface in situ
71	McMurdo Station, Antarctica	United States	04.12.1985	Terminated 28.10.1987	Surface Flasks *
72	High Altitude Global Climate Observation Center	Mexico	09.01.2009	ongoing	Surface Flasks
73	Mace Head, County Galway	Ireland	03.06.1991	ongoing	Surface Flasks
74	Sand Island, Midway	United States	03.05.1985	ongoing	Surface Flasks
75	Mt. Kenya	Kenya	23.12.2003	Terminated 21.06.2011	Surface Flasks *
76	Mauna Kea, Hawaii	United States	N/A	N/A	Surface Flasks *
77	Mauna Loa, Hawaii	United States	N/A	N/A	Surface Flasks *

Table A3. *Cont.*

Site	Name	Location	First Carbon Dioxide Dataset	Status Carbon Dioxide Dataset	Air Sample Collection Method
78	Mauna Loa, Hawaii	United States	20.08.1969	ongoing	In Situ Observatory Surface Flasks
79	Marcellus Pennsylvania	United States	03.08.2015	ongoing	Airborne Flasks * Surface Flasks
80	Mashpee, Massachusetts	United States	11.05.2016	ongoing	Surface Flasks
81	Marthas Vineyard, Massachusetts	United States	27.04.2007	Terminated 04.03.2011	Surface Flasks *
82	Mt. Wilson Observatory	United States	30.04.2010	ongoing	Surface Flasks
83	Farol De Mae Luiza Lighthouse	Brazil	12.09.2010	Terminated 11.03.2020	Surface Flasks *
84	NE Baltimore, Maryland	United States	04.04.2018	ongoing	Surface Flasks
85	Offshore Portsmouth, New Hampshire (Isles of Shoals)	United States	12.09.2003	ongoing	Airborne Flasks
86	Gobabeb	Namibia	13.01.1997	ongoing	Surface Flasks
87	NW Baltimore	United States	17.04.2018	ongoing	Surface Flasks
88	Niwot Ridge Forest, Colorado	United States	20.01.2006	Terminated 08.11.2009	Surface Flasks *
89	Niwot Ridge, Colorado	United States	18.05.1967 16.09.2005	ongoing ongoing	Airborne Flasks * Surface Flasks
90	Kaitorete Spit	New Zealand	26.10.1982	Terminated 09.04.1985	Surface Flasks *
91	Oglesby, Illinois	United States	16.09.2004	Terminated 19.11.2005	Airborne Flasks *
92	Olympic Peninsula, Washington	United States	06.01.1984	Terminated 30.05.1990	Surface Flasks *
93	Ochsenkopf	Germany	13.03.2003	Terminated 04.06.2019	Surface Flasks *
94	Pallas-Sammaltunturi, GAW Station	Finland	21.12.2001	ongoing	Surface Flasks
95	Pico, Azores	Portugal	02.08.2010	Terminated 18.07.2011	Surface Flasks *
96	Poker Flat, Alaska	United States	27.06.1999	ongoing	Airborne Flasks
97	Pacific Ocean (0 N)	N/A	20.12.1986	Terminated 10.07.2017	Surface Flasks *
98	Pacific Ocean (5 N)	N/A	19.12.1986	Terminated 11.07.2011	Surface Flasks *

Table A3. *Cont.*

Site	Name	Location	First Carbon Dioxide Dataset	Status Carbon Dioxide Dataset	Air Sample Collection Method
99	Pacific Ocean (10 N)	N/A	14.01.1987	Terminated 12.07.2017	Surface Flasks *
100	Pacific Ocean (15 N)	N/A	17.12.1986	Terminated 13.07.2017	Surface Flasks *
101	Pacific Ocean (20 N)	N/A	16.12.1986	Terminated 14.07.2017	Surface Flasks *
102	Pacific Ocean (25 N)	N/A	15.12.1986	Terminated 15.07.2017	Surface Flasks *
103	Pacific Ocean (30 N)	N/A	14.12.1986	Terminated 16.07.2017	Surface Flasks *
104	Pacific Ocean (35 N)	N/A	21.01.1987	Terminated 18.06.2007	Surface Flasks *
105	Pacific Ocean (40 N)	N/A	04.06.1987	Terminated 14.08.1996	Surface Flasks *
106	Pacific Ocean (45 N)	N/A	05.06.1987	Terminated 15.08.1996	Surface Flasks *
107	Pacific Ocean (5 S)	N/A	21.12.1986	Terminated 09.07.2017	Surface Flasks *
108	Pacific Ocean (10 S)	N/A	22.12.1986	Terminated 08.07.2017	Surface Flasks *
109	Pacific Ocean (15 S)	N/A	25.12.1986	Terminated 07.07.2017	Surface Flasks *
110	Pacific Ocean (20 S)	N/A	28.12.1986	Terminated 05.07.2017	Surface Flasks *
111	Pacific Ocean (25 S)	N/A	29.12.1986	Terminated 04.07.2017	Surface Flasks *
112	Pacific Ocean (30 S)	N/A	29.12.1986	Terminated 03.07.2017	Surface Flasks *
113	Pacific Ocean (35 S)	N/A	30.12.1986	Terminated 03.01.2012	Surface Flasks *
114	Palmer Station, Antarctica	United States	27.01.1978	ongoing	Surface Flasks
115	Point Six Mountain, Montana	United States	28.04.1978	Terminated 24.12.1982	Surface Flasks *
116	Point Arena, California	United States	05.01.1999	Terminated 25.05.2011	Surface Flasks *
117	Ragged Point	Barbados	14.11.1987	ongoing	Surface Flasks
118	Rarotonga	Cook Islands	16.04.2000	ongoing	Airborne Flasks
119	Santarem	Brazil	07.12.2000	Terminated 20.08.2003	Airborne Flasks *
120	Offshore Charleston, South Carolina	United States	22.08.2003	ongoing	Airborne Flasks
121	South China Sea (3 N)	N/A	05.07.1991	Terminated 07.10.1998	Surface Flasks *
122	South China Sea (6 N)	N/A	05.07.1991	Terminated 09.10.1998	Surface Flasks *
123	South China Sea (9 N)	N/A	06.07.1991	Terminated 10.10.1998	Surface Flasks *

Table A3. *Cont.*

Site	Name	Location	First Carbon Dioxide Dataset	Status Carbon Dioxide Dataset	Air Sample Collection Method
124	South China Sea (12 N)	N/A	06.07.1991	Terminated 10.10.1998	Surface Flasks *
125	South China Sea (15 N)	N/A	07.07.1991	Terminate 15.10.1998	Surface Flasks *
126	South China Sea (18 N)	N/A	08.07.1991	Terminated 14.10.1998	Surface Flasks *
127	South China Sea (21 N)	N/A	08.07.1991	Terminated 14.10.1998	Surface Flasks *
128	Beech Island, South Carolina	United States	14.08.2008	ongoing	in Situ Observatory Surface Flasks
129	Shangdianzi	China	03.09.2009	Terminated 02.09.2015	Surface Flasks *
130	Mahe Island	Seychelles	15.01.1980	ongoing	Surface Flasks
131	Bird Island, South Georgia	United Kingdom	02.02.1989	Terminated 13.08.1992	Surface Flasks *
132	Southern Great Plains, Oklahoma	United States	02.04.2002 29.10.2010	ongoingongoing	Airborne Flasks Surface Flasks
133	Shemya Island, Alaska	United States	04.09.1985	ongoing	Surface Flasks
134	La Jolla, California	United States	01.01.1968	Terminated 25.09.1986	Surface Flasks *
135	Tutuila	American Samoa	15.01.1972	ongoing	in Situ Observatory Surface Flasks
136	Shenandoah National Park	United States	26.08.2008	ongoing	Surface in Situ
137	South Pole, Antarctica	United States	21.01.1975	ongoing	in Situ Observatory Surface Flasks
138	Ocean Station Charlie	United States	21.11.1968	Terminated 12.05.1973	Surface Flasks *
139	Ocean Station M	Norway	08.03.1981	Terminated 27.11.2009	Surface Flasks *
140	Sutro Tower, San Francisco, California	United States	02.10.2007	ongoing	Surface Flasks
141	Summit	Greenland	23.06.1997	ongoing	Surface Flasks
142	Syowa Station, Antarctica	Japan	25.01.1986	ongoing	Surface Flasks
143	Tacolneston	United Kingdom	06.06.2014	Terminated 04.01.2016	Surface Flasks *
144	Tae-ahn Peninsula	Republic of Korea	24.11.1990	ongoing	Surface Flasks
145	Tambopata	Peru	N/A	N/A	Surface in Situ

Table A3. *Cont.*

Site	Name	Location	First Carbon Dioxide Dataset	Status Carbon Dioxide Dataset	Air Sample Collection Method
146	Offshore Corpus Christi, Texas	United States	09.09.2003	ongoing	Airborne Flasks
147	Trinidad Head, California	United States	19.04.2002	Terminated 01.06.2017	Airborne Flasks Surface Flasks *
148	Hydrometeorological Observatory of Tiksi	Russia	15.08.2011	Terminated 03.09.2018	Surface Flasks *
149	Thurmont, Maryland	United States	01.08.2017	ongoing	Surface Flasks
150	Taiping Island	Taiwan	28.05.2019	ongoing	Surface Flasks
151	Ulaanbaatar	Mongolia	25.03.2004	Terminated 05.03.2009	Airborne Flasks *
152	Ushuaia	Argentina	14.09.1994	ongoing	Surface Flasks
153	Wendover, Utah	United States	06.05.1993	ongoing	Surface Flasks
154	Ulaan Uul	Mongolia	01.01.1992	ongoing	Surface Flasks
155	West Branch, Iowa	United States	28.06.2007	ongoing	In Situ Tall Tower Airborn Flasks Surface Flasks
156	Walnut Grove, California	United States	20.09.2007	ongoing	In Situ Tall Tower Airborne Flasks * Surface Flasks
157	Weizmann Institute of Science at the Arava Institute, Ketura	Israel	27.11.1995	ongoing	Surface Flasks
158	Moody, Texas	United States	11.02.2001 07.07.2006	Terminated 01.10.2010 ongoing	In Situ Tall Tower Surface Flasks
159	Mt. Waliguan	Peoples Republic of China	05.08.1990	ongoing	Surface Flasks
160	Western Pacific Cruise (0 N)	N/A	10.05.2004	Terminated 27.05.2013	Surface Flasks *
161	Western Pacific Cruise (5 N)	N/A	11.05.2004	Terminated 29.05.2013	Surface Flasks *
162	Western Pacific Cruise (10 N)	N/A	11.05.2004	Terminated 29.05.2013	Surface Flasks *
163	Western Pacific Cruise (15 N)	N/A	12.05.2004	Terminated 30.05.2013	Surface Flasks *
164	Western Pacific Cruise (20 N)	N/A	12.05.2004	Terminated 31.05.2013	Surface Flasks *
165	Western Pacific Cruise (25 N)	N/A	13.05.2003	Terminated 01.06.2013	Surface Flasks *

Table A3. *Cont.*

Site	Name	Location	First Carbon Dioxide Dataset	Status Carbon Dioxide Dataset	Air Sample Collection Method
166	Western Pacific Cruise (30 N)	N/A	14.05.2004	Terminated 01.06.2013	Surface Flasks *
167	Western Pacific Cruise (5 S)	N/A	09.05.2004	Terminated 27.05.2013	Surface Flasks *
168	Western Pacific Cruise (10 S)	N/A	08.05.2004	Terminated 26.05.2013	Surface Flasks *
169	Western Pacific Cruise (15 S)	N/A	08.05.2004	Terminated 25.05.2013	Surface Flasks *
170	Western Pacific Cruise (20 S)	N/A	07.05.2004	Terminated 25.05.2013	Surface Flasks *
171	Western Pacific Cruise (25 S)	N/A	06.05.2004	Terminated 24.05.2013	Surface Flasks *
172	Western Pacific Cruise (30 S)	N/A	05.05.2004	Terminated 23.05.2013	Surface Flasks *
173	Ny-Alesund, Svalbard	Norway and Sweden	11.02.1994	ongoing	Surface Flasks

*—Indicates discontinued site or project.

Table A4. Comparison of satellite data and TCCON stations.

No.	Location	Coordination	Period	Satellite Name	Satellite Difference with Ground Station	Number of Observations	Note		Reference
1	China	NH	2010 to 2016	GOSAT	−1.04 ± 2.10 ppm	chinese text	correlation coefficient of 0.90		Deng A. et al., 2020 [142]
2	27 TCCON stations		July 2009–May 2016	GOSAT	0.24 ± 1.68 ppm	1913 NH 575 SH	0.349 ± 1.699 ppm NH −0.128 ± 1.561 ppm SH	2488 matched observations	Yawen Kong et al., 2019 [143]
			September 2014–July 2017	OCO-2	0.34 ± 1.57 ppm	779 NH 294 SH	0.283 ± 1.584 ppm NH 0.494 ± 1.127 ppm SH	1073 matched observations	
3	Tsukuba	36.05° N, 140.12° E	September 2014–August 2016	GOSAT	0.07± 2.36 ppm	N/A			Qin et al., 2019 [48]
4	Various TCCON stations	Both Hemisphere	September 2014 and July 2016	OCO-2	−0.02 ± 1.36 ppm	34,560	RemoTeC algorithm version 7 data		Lianghai Wu et al., 2018 [144]
5	Burgos, Ilocos Norte, Philippines	18.52° N, 120.65° E	2017	GOSAT	−0.86 ± 1.06 ppm	N/A			Voltaire A. Velazco et al., 2017 [145]
				OCO-2	−0.83 ± 1.22 ppm	164			

Table A4. *Cont.*

No.	Location	Coordination	Period	Satellite Name	Satellite Difference with Ground Station	Number of Observations	Note		Reference
6	Various TCCON stations			OCO-2	0.4± 1.50 ppm	2790			Wunch et al., 2017 [41]
7	global TCCON stations			GOSAT	0.01 ± 1.22 ppm				Zhao-Cheng Zeng et al., 2017 [56]
8	Various TCCON stations	Both Hemisphere	2009–2016	GOSAT	−0.4107 ± 2.216 ppm	1813 NH 596 SH	−0.214 ± 2.009 ppm NH −1.016 ± 1.956 ppm SH		Ailin Liang et al., 2017 [146]
			2014–2016	GOSAT	−0.62 ± 2.3 ppm	563 NH 151 SH	−0.312 ± 2.006 ppm NH −1.778 ± 2.096 ppm SH		
			September 2014 to December 2016	OCO-2	0.2671 ± 1.56 ppm	730 NH 321 SH	0.175 ± 1.402 ppm NH 0.476 ± 1.065 ppm SH		
9	11 TCCON stations	Both Hemisphere	2009–2014	GOSAT	0.73 ± 1.83 ppm	1484 NH 634 SH	0.959 ± 1.724 ppm NH 0.209 ± 1.706 ppm SH	Photon path length Probability Density Function-Simultaneous (PPDF-S) retrieval method	Chisa Iwasaki et al., 2017 [147]
				GOSAT	−0.32 ± 2.16 ppm	1484 NH 634 SH	−0.299 ± 1.860 ppm NH −0.384 ± 2.104 ppm SH	standard products for General Users (GU) of XCO2	
10	Tsukuba and Saga	NH		GOSAT	1.25 ± 2.12 ppm	207	NIES algorithm		Woogyung Kim et al., 2016 [69]
				GOSAT	1.94 ± 1.89 ppm	205	ACOS algorithm		
11	Various TCCON stations		September 2014–November 2015	OCO-2	0.87 ± 1.8 ppm	not provided in the paper			Liang A. et al., 2016 [148]

Table A4. *Cont.*

No.	Location	Coordination	Period	Satellite Name	Satellite Difference with Ground Station	Number of Observations	Note		Reference
12	11 TCCON stations	45° S–80° N	June 2009–April 2014	GOSAT	±1.7 ppm	not provided in the paper	ACOS b3.5		Susan Kulawik et al., 2016 [149]
		45° S–80° N	January 2003–April 2012	ENVISAT (SCIAMACHY)	±2.1 ppm	not provided in the paper	Bremen Optimal Estimation DOAS, BESD v2.00.08		
13	12 TCCON stations		2010 to 2012	GOSAT	0.21 ± 1.85 ppm	2409 NH 915 SH	0.062 ± 1.815 ppm NH 0.597 ± 1.684 ppm SH	ACOS data	Anjian Deng et al., 2016 [150]
			2010 to 2012	GOSAT	−0.69 ± 2.13 ppm	407 NH 191 SH	−0.679 ± 2.103 ppm NH −0.720 ± 1.401 ppm SH	NIES data (National Institute for Environmental Studies of Japan)	
14	Izaña Ascension Island Darwin Reunion Island Wollongong	28.3° N, 16.5° W 7.9° S, 14.3° W 12.4° S, 130.9° E 20.9° S, 55.5° E 34.4° S, 150.8° E	April 2009–May 2014	GOSAT	−0.184 ± 0.028 ppm	1137 NH 5877 SH	−0.064 ± 0.032 ppm NH −0.207 ± 0.027 ppm SH	NIES version 02.21	Minqiang Zhou et al., 2016 [151]
			April 2009–December 2013	GOSAT	0.038 ± 0.032 ppm	726 NH 6532 SH	0.057 ± 0.056 ppm NH 0.035 ± 0.028 ppm SH	SRON/KIT algorithm, SRFP v2.3.5	
			April 2009–June 2014	GOSAT	−0.006 ± 0.019 ppm	1519 NH 8960 SH	−0.001 ± 0.026 ppm NH −0.007 ± 0.018 ppm SH	ACOS version 3.5	
15	TCCON stations			GOSAT	0.15 ± 1.48 ppm	not provided in the paper	modification of the algorithm from Institute of Atmospheric Physics, Chinese Academy of Sciences		Dongxu Yang et al., 2015 [70]
16	Various TCCON stations		2004–2013	GOSAT	−0.38 ± 1.992 ppm	5522 NH 1530 SH	−0.364 ± 2.078 ppm NH −0.439 ± 1.640 ppm SH	Bremen Optimal Estimation DOAS (BESD) algorithm	J. Heymann et al., 2015 [152]
				ENVISAT (SCIAMACHY)	−0.105 ± 2.017 ppm	32,619 NH 15,336 SH	−0.071 ± 2.097 ppm NH −0.179 ± 1.836 ppm SH		

Table A4. *Cont.*

No.	Location	Coordination	Period	Satellite Name	Satellite Difference with Ground Station	Number of Observations	Note		Reference
17	Eureka, Park Falls, Lamont, Sodankyla, Bialystok, Orleans and Garmisch	NH	April 2010 to March 2012	GOSAT	−0.94 ± 2.26 ppm	659	ACOS		ZHANG Miao et al., 2014 [153]
				GOSAT	−1.49 ± 2.27 ppm	755	NIES		
				ENVISAT	−1.52 ± 2.91 ppm	378	SCIAMACHY		
18	Various TCCON stations			GOSAT	−8.85 ± 4.75 ppm	62	SWIR L2 product version 01.xx	The old version with low accuracy and precision (neglected in calculations and figure)	I. Morino et al., 2011 [154] Y. Yoshida et al., 2013 [155]
			April 2009 to May 2011	GOSAT	−1.48 ± 2.09 ppm	567 NH 152 SH	−1.485 ± 1.734 ppm NH −1.447 ± 2.276 ppm SH	SWIR L2 product version 02.xx 719 observations	
19	Bialystok, Bremen, Orleans, Park falls, Lamont, Darwin, Wollongong		2009–2011	GOSAT	−0.20 ± 2.26 ppm	467 NH 110 SH	0.214 ± 2.197 ppm NH −0.035 ± 2.391 ppm SH	577 observations	A. J. Cogan et al., 2012 [156]
20	Bialystok, Orleans, Park Falls, Lamont, Darwin, Wollongong		April 2009 and July 2010	GOSAT	−0.05 ± 0.37% −0.203 ± 2.654 ppm	759 NH 128 SH	−0.528 ± 2.586 ppm NH 1.721 ± 3.029 ppm SH	TANSO-FTS 887 observation	A. Butz et al., 2011 [157]

NH = Northern Hemisphere, SH = Sothern Hemisphere.

Table A5. worldwide ground-based station.

No.	Location	Coordination	Elevation * a.s.l.: above Sea Level	Period	Instrument	Note	Reference
1	Bharati, the Indian Antarctic research station	69.24° S, 76.11° E	35 m a.s.l. *	austral summer (January–February) of 2016	Li-Cor CO2/H2O analyzer (model Li-840A)		Mahesh Patakothi et al., 2018 [97]
2	Bahir Dar and Hawassa	11°36′ N, 37°23′ E 07°15′ N, 38°45′ E	1786–1886 m 1708 m a.s.l.		Aeroqual Series 500 portable gas monitor and YuanTe SKY 2000-M4 handheld multi-gas detector	correlation coefficient between instrument was 0.986	Oluwasinaayomi Faith Kasim et al., 2018 [158]
3	Peterhof station (St. Petersburg, Russia)	59.88° N, 29.82° E		2009–2017	Fourier transform IR spectrometry (FTIR) using a Bruker 125HR	total error of 4.18 ± 0.02%, with 0.36 ± 0.06% and 4.16 ± 0.02% for random and systematic errors respectively	Virolainen Ya. A. 2018 [159]
4	Hefei, China	31°54′ N, 117°10′ E	29 m a.s.l.	July 2014–April 2016	Bruker IFS 125HR spectrometer and solar tracker InGaAs detector from July 2015	similar variation phase and seasonal amplitude with Tsukuba TCCON station	Wei Wang et al., 2017 [160]
5	Ny-Ålesund	78.92° N, 11.92° E		2005–2015	Bruker IFS 120HR FTIR spectrometer	lower sensitivity in the troposphere in comparison to TCCON (by a factor of 2)	Matthias Buschmann et al., 2016 [161]
6	Karlsruhe	49.094° N, 8.4336° E	133 m a.s.l.	3 February 2012–22 June 2012	EM27 spectrometer	commercial low-resolution (0.5 cm−1) (FTS) agreement with Karlsruhe TCCON station, (0.12 ± 0.08)%	Gisi M. et al., 2012 [162]
7	China: Lin'an, Longfengshan, Shangdianzi, and Waliguan			January 2009 to December 2011	cavity ring-down spectroscopy systems (G1301, Picarro Inc.)	according to Chen et al., 2010; Crosson, 2008, this type of instrument is suitable for making precise measurement	S. X. Fang et al., 2014 [115]
8	Kitt Peak, Arizona	31.9° N, 111.6° W	2070 m a.s.l.	1977–1995	Fourier transform spectrometer on the McMath telescope.	precisions better than 0.5% similar behavior to the Mauna Loa	Zhonghua Yang et al., 2002 [163]

Table A5. *Cont.*

No.	Location	Coordination	Elevation * a.s.l.: above Sea Level	Period	Instrument	Note	Reference
9	Tsukuba, Meteorological Research Institute	36°04′ N, 140°07′ E	25 m a.s.l.	1986–1996	NDIR analyzer (Beckman model 864) from 1986–1992 NDIR analyzer (Beckman model 880) from 1992–1994		Hisayuki Yoshikawa Inoue and Hidekadzu Matsueda 1996 [164]
10	Mt. Cimone Station, Italy	44°11′ N, 10°42′ E	2165 m a.s.l.	1979–1992	URAS-2T NDIR analyzer, from 1979 ULTRAMAT-5E NDIR from 1988 URAS-3G NDIR (to control)	URAS-2T NDIR precision is ±0.3 p.p.m.v. ULTRAMAT-5E NDIR precision is ±0.1 p.p.m.v.	V.Cundari et al. 1995 [165]
11	Izaña, Tenerife, Canary Islands	28°18′ N, 16°29′ W	2367 m a.s.l.	1984–1988	Siemens Ultramat-3 NADIR	the samples were representative of free troposphere in the southern part of the North Atlantic because of the high altitude of the location	Beatriz Navascués et al. 1991 [166]
12	Amsterdam island	37°47′ S, 77°31′ E		1980–1989	non-dispersive infrared analyzer URAS 2T		A. Gaudry et al. 1991 [167]
13	La Jolla, California Mauna Loa, Hawaii Cape Kumukahi, Hawaii Fanning island and South pole	32.9° N, 117.3° W 19.5° N, 155.6° W 19.5° N, 154.8° W 3.9° N, 159.3° W 90° S, 59° E		March 1977–February 1982	non-dispersive infrared gas analyzer		Illem g. Mook and Marjan Koopmans 1983 [168]
14	Shetland Isles, Scotland	60.2° N, 1.2° W		1992–1996	Carle Series 400 gas chromatograph Finnigan MAT 252 mass spectrometer with MT Box-C gas preparationsystem	a part of CSIRO network	R.J. Francey et al. 1998 [169]

Table A5. *Cont.*

No.	Location	Coordination	Elevation * a.s.l.: above Sea Level	Period	Instrument	Note	Reference
15	Schauinsland station, southwest Germany	47°55′ N, 7°55′ E	1205 m a.s.l.	1972–2002	nondispersive infrared analysis (NDIR) Until August 1980,URAS-2 (Hartmann & Braun), from September 1980 until the end of 1993,Ultramat-3 (Siemens) and from 1994 onward with URAS-3 (Hartmann & Braun)	The accuracy of the data was estimated: better than ±1 ppm for the period 1972–1991 and better than ±0.5 ppm later on.	M. Schmidt et al., 2003 [170]
16	Kasprowy Wierch Kraków in southern Poland	49°14′ N, 19°59′ E 50°04′ N, 19°55′ E	1989 m a.s.l. 220 m a.s.l.	1996–2006	Automated gas chromatographs (Hewlett Packard, Series 5890, with FID detector and Ni catalyst for conversion of CO2 to CH4 and Porapak Q column)		L. Chmura et al., 2008 [171]
17	Moscow to Khabarovsk			1997–2004	LI6262 gas analyzer (LICOR, United States)	mobile measurement at surface layer with the error of ±1 ppm at a CO2 concentration of 350 ppm. The intrinsic noise was 0.2 ppm	I. B. Belikov et al., 2006 [172]
18	ZOTTO international observatory, Krasnoyarsk krai, Russia	60° N, 90° E	114 m a.s.l.	January 2006-December 2013	NDIR CO2 Analyzer (Siemens AG, Ultramat 6F) up to April 2007 EnviroSense 3000i gas-analyzing system (Picarro Inc., USA) from May 2009	using the tall tower (302 m) measurement error does not exeed 0.1 ppm	A. V. Timokhina et al., 2015 [173] E. A. Kozlova and A. C. Manning 2009 [174]
19	Cabauw	51.971° N, 4.927° E	−0.7 m a.s.l.	1992–2010	Siemens Ultramat NDIR 1992–2004 NDIR (LICOR 7000) after 2004	sampling in tall tower Siemens Ultramat NDIR resolution in the range of 0–500 ppm was 0.5 ppm	A. T. Vermeulen et al., 2011 [175]

Table A5. *Cont.*

No.	Location	Coordination	Elevation * a.s.l.: above Sea Level	Period	Instrument	Note	Reference
20	Barrow (Alaska)	71.32° N, 156.61° W	11.00 m a.s.l.	stablished in 1973	non-dispersive infrared analyzer		https://www.esrl.noaa.gov/gmd/obop/brw/ (accessed on 16 August 2021)
21	American Samoa	14.24° S, 170.56° W	42.00 m a.s.l.	stablished in 1974	non-dispersive infrared analyzer		https://www.esrl.noaa.gov/gmd/obop/smo/ (accessed on 16 August 2021) https://cdiac.ess-dive.lbl.gov/trends/co2/sio-sam.html (accessed on 16 August 2021)
22	South Pole	90° S, 59° E	2837 m a.s.l.	stablished in 1957	non-dispersive infrared gas analyzer		https://www.esrl.noaa.gov/gmd/obop/spo/ (accessed on 16 August 2021) Illem g. Mook and Marjan Koopmans 1983 [168]
23	Ascension Island (SH)	7.92° S, 14.33° W	10 m a.s.l.	Available data from 22.05.2012–31.10.2018		TCCON station	https://tccondata.org/ (accessed on 16 August 2021) https://tccon-wiki.caltech.edu/Main/TCCONSites (accessed on 16 August 2021)

Table A5. *Cont.*

No.	Location	Coordination	Elevation * a.s.l.: above Sea Level	Period	Instrument	Note	Reference
24	Anmeyondo (KR)	36.54° N, 126.33° E	30 m a.s.l.	Available data from 02.02.2015–18.04.2018		TCCON station	https://tccondata.org/ (accessed on 16 August 2021) https://tccon-wiki.caltech.edu/Main/TCCONSites (accessed on 16 August 2021)
25	Bialystok (PL)	53.23° N, 23.025° E	180 m a.s.l.	Available data from 01.03.2009–01.10.2018		TCCON station	https://tccondata.org/ (accessed on 16 August 2021) https://tccon-wiki.caltech.edu/Main/TCCONSites (accessed on 16 August 2021)
26	Bremen (DE)	53.10° N, 8.85° E	27 m a.s.l.	Available data from 22.01.2010–23.08.2019		TCCON station	https://tccondata.org/ (accessed on 16 August 2021) https://tccon-wiki.caltech.edu/Main/TCCONSites (accessed on 16 August 2021)

Table A5. *Cont.*

No.	Location	Coordination	Elevation * a.s.l.: above Sea Level	Period	Instrument	Note	Reference
27	Burgos	18.533° N, 120.650° E	35 m a.s.l.	Available data from 03.03.2017–31.01.2020		TCCON station	https://tccondata.org/ (accessed on 16 August 2021) https://tccon-wiki.caltech.edu/Main/TCCONSites (accessed on 16 August 2021)
28	Caltech (US)	34.136° N, 118.127° W	230 m a.s.l.	Available data from 20.09.2012–03.10.2020		TCCON station	https://tccondata.org/ (accessed on 16 August 2021) https://tccon-wiki.caltech.edu/Main/TCCONSites (accessed on 16 August 2021)
29	Darwin (AU)	12.42° S, 130.89° E 12.46° S, 130.93° E	30 m a.s.l. 37 m a.s.l.	Available data from 28.08.2005–31.01.2020		TCCON station	https://tccondata.org/ (accessed on 16 August 2021) https://tccon-wiki.caltech.edu/Main/TCCONSites (accessed on 16 August 2021)

Table A5. *Cont.*

No.	Location	Coordination	Elevation * a.s.l.: above Sea Level	Period	Instrument	Note	Reference
30	Edwards (US)			Available data from 20.07.2013–03.10.2020		TCCON station	https://tccondata.org/ (accessed on 16 August 2021) https://tccon-wiki.caltech.edu/Main/TCCONSites (accessed on 16 August 2021)
31	East Trout Lake	54.35° N, 104.99° W	501.8 m a.s.l.	Available data from 07.10.2016–06.09.2020		TCCON station	https://tccondata.org/ (accessed on 16 August 2021) https://tccon-wiki.caltech.edu/Main/TCCONSites (accessed on 16 August 2021)
32	Eureka (CA)	80.05° N, 86.42° W	610 m a.s.l.	Available data from 24.07.2010–06.07.2020		TCCON station	https://tccondata.org/ (accessed on 16 August 2021) https://tccon-wiki.caltech.edu/Main/TCCONSites (accessed on 16 August 2021)

Table A5. *Cont.*

No.	Location	Coordination	Elevation * a.s.l.: above Sea Level	Period	Instrument	Note	Reference
33	Four Corners (US)	36.80° N, 108.48° W	1643 m a.s.l.	Available data from 16.03.2013–04.10.2013		TCCON station	https://tccondata.org/ (accessed on 16 August 2021) https://tccon-wiki.caltech.edu/Main/TCCONSites (accessed on 16 August 2021)
34	Garmisch (DE)	47.476° N, 11.063° E	740 m a.s.l.	Available data from 16.07.2007–18.10.2019		TCCON station	https://tccondata.org/ (accessed on 16 August 2021) https://tccon-wiki.caltech.edu/Main/TCCONSites (accessed on 16 August 2021)
35	Hefei (PRC)	31.90° N, 118.67° E	29 m a.s.l.	Available data from 18.09.2015–31.12.2016		TCCON station	https://tccondata.org/ (accessed on 16 August 2021) https://tccon-wiki.caltech.edu/Main/TCCONSites (accessed on 16 August 2021)

Table A5. *Cont.*

No.	Location	Coordination	Elevation * a.s.l.: above Sea Level	Period	Instrument	Note	Reference
36	Indianapolis (US)	39.86° N, 86.00° W	270 m a.s.l.	Available data from 23.08.2012–01.12.2012		TCCON station	https://tccondata.org/ (accessed on 16 August 2021) https://tccon-wiki.caltech.edu/Main/TCCONSites (accessed on 16 August 2021)
37	Izana (ES)	28.3° N, 16.5° W	2370 m a.s.l.	Available data from 18.05.2007–02.11.2020		TCCON station	https://tccondata.org/ (accessed on 16 August 2021) https://tccon-wiki.caltech.edu/Main/TCCONSites (accessed on 16 August 2021)
38	Jet Propulsion Laboratory (US)	34.20° N, 118.175° W	390 m a.s.l.	Available data from 31.07.2007–22.06.2008		TCCON station	https://tccondata.org/ (accessed on 16 August 2021) https://tccon-wiki.caltech.edu/Main/TCCONSites (accessed on 16 August 2021)

Table A5. *Cont.*

No.	Location	Coordination	Elevation * a.s.l.: above Sea Level	Period	Instrument	Note	Reference
39	Jet Propulsion Laboratory (US)	34.20° N, 118.175° W	390 m a.s.l.	Available data from 19.05.2011–14.05.2018		TCCON station	https://tccondata.org/ (accessed on 16 August 2021) https://tccon-wiki.caltech.edu/Main/TCCONSites (accessed on 16 August 2021)
40	Saga (JP)	33.24° N, 130.29° E	7 m a.s.l.	Available data from 28.07.2011–04.08.2020		TCCON station	https://tccondata.org/ (accessed on 16 August 2021) https://tccon-wiki.caltech.edu/Main/TCCONSites (accessed on 16 August 2021)
41	Karlsruhe (DE)	49.10° N, 8.44° E	116 m a.s.l.	Available data from 19.04.2010–31.10.2020		TCCON station	https://tccondata.org/ (accessed on 16 August 2021) https://tccon-wiki.caltech.edu/Main/TCCONSites (accessed on 16 August 2021)

Table A5. *Cont.*

No.	Location	Coordination	Elevation * a.s.l.: above Sea Level	Period	Instrument	Note	Reference
42	Lauder (NZ)	45.04° S, 169.68° E	370 m a.s.l.	Available data from 29.06.2004–09.12.2010		TCCON station	https://tccondata.org/ (accessed on 16 August 2021) https://tccon-wiki.caltech.edu/Main/TCCONSites (accessed on 16 August 2021)
43	Lauder (NZ)	45.04° S, 169.68° E	370 m a.s.l.	Available data from 02.02.2010–31.10.2018		TCCON station	https://tccondata.org/ (accessed on 16 August 2021) https://tccon-wiki.caltech.edu/Main/TCCONSites (accessed on 16 August 2021)
44	Lauder (NZ)	45.04° S, 169.68° E	370 m a.s.l.	Available data from 03.10.2018–31.07.2020		TCCON station	https://tccondata.org/ (accessed on 16 August 2021) https://tccon-wiki.caltech.edu/Main/TCCONSites (accessed on 16 August 2021)

Table A5. *Cont.*

No.	Location	Coordination	Elevation * a.s.l.: above Sea Level	Period	Instrument	Note	Reference
45	Manaus (BR)	3.21° S, 60.59° W	50 m a.s.l.	Available data from 01.10.2014–24.06.2015		TCCON station	https://tccondata.org/ (accessed on 16 August 2021) https://tccon-wiki.caltech.edu/Main/TCCONSites (accessed on 16 August 2021)
46	Nicosia	35.14° N, 33.38° E	185 m a.s.l.	Available data from 31.08.2019–31.01.2020		TCCON station	https://tccondata.org/ (accessed on 16 August 2021) https://tccon-wiki.caltech.edu/Main/TCCONSites (accessed on 16 August 2021)
47	Lamont (US)	36.60° N, 97.48° W	320 m a.s.l.	Available data from 06.07.2008–03.10.2020		TCCON station	https://tccondata.org/ (accessed on 16 August 2021) https://tccon-wiki.caltech.edu/Main/TCCONSites (accessed on 16 August 2021)

Table A5. *Cont.*

No.	Location	Coordination	Elevation * a.s.l.: above Sea Level	Period	Instrument	Note	Reference
48	Orléans (FR)	47.97° N, 2.11° E	130 m a.s.l.	Available data from 29.08.2009–18.09.2019		TCCON station	https://tccondata.org/ (accessed on 16 August 2021) https://tccon-wiki.caltech.edu/Main/TCCONSites (accessed on 16 August 2021)
49	Park Falls (US)	45.94° N, 90.27° W	440 m a.s.l.	Available data from 02.06.2004–03.10.2020		TCCON station	https://tccondata.org/ (accessed on 16 August 2021) https://tccon-wiki.caltech.edu/Main/TCCONSites (accessed on 16 August 2021)
50	Paris (FR)	48.84° N, 2.35° E	60 m a.s.l.	Available data from 23.09.2014–24.01.2020		TCCON station	https://tccondata.org/ (accessed on 16 August 2021) https://tccon-wiki.caltech.edu/Main/TCCONSites (accessed on 16 August 2021)

Table A5. *Cont.*

No.	Location	Coordination	Elevation * a.s.l.: above Sea Level	Period	Instrument	Note	Reference
51	Réunion Island (RE)	20.90° S, 55.48° E	87 m a.s.l.	Available data from 16.09.2011–18.07.2020		TCCON station	https://tccondata.org/ (accessed on 16 August 2021) https://tccon-wiki.caltech.edu/Main/TCCONSites (accessed on 16 August 2021)
52	Rikubetsu (JP)	43.45° N, 143.77° E	380 m a.s.l.	Available data from 16.11.2013–30.09.2019		TCCON station	https://tccondata.org/ (accessed on 16 August 2021) https://tccon-wiki.caltech.edu/Main/TCCONSites (accessed on 16 August 2021)
53	Sodankylä (FI)	67.37° N, 26.63° E	188 m a.s.l.	Available data from 16.05.2009–30.09.2020		TCCON station	https://tccondata.org/ (accessed on 16 August 2021) https://tccon-wiki.caltech.edu/Main/TCCONSites (accessed on 16 August 2021)

Table A5. *Cont.*

No.	Location	Coordination	Elevation * a.s.l.: above Sea Level	Period	Instrument	Note	Reference
54	Ny Ålesund	78.9° N, 11.9° E	20 m a.s.l.	Available data from 06.04.2014–15.09.2019		TCCON station	https://tccondata.org/ (accessed on 16 August 2021) https://tccon-wiki.caltech.edu/Main/TCCONSites (accessed on 16 August 2021)
55	Tsukuba (JP)	36.05° N, 140.12° E	30 m a.s.l.	Available data from 04.08.2011–30.09.2019		TCCON station	https://tccondata.org/ (accessed on 16 August 2021) https://tccon-wiki.caltech.edu/Main/TCCONSites (accessed on 16 August 2021)
56	Wollongong (AU)	34.41° S, 150.88° E	30 m a.s.l.	Available data from 26.06.2008–31.01.2020		TCCON station	https://tccondata.org/ (accessed on 16 August 2021) https://tccon-wiki.caltech.edu/Main/TCCONSites (accessed on 16 August 2021)

Table A5. *Cont.*

No.	Location	Coordination	Elevation * a.s.l.: above Sea Level	Period	Instrument	Note	Reference
57	Zugspitze (DE)	47.42° N, 10.98° E	2960 m a.s.l.	Available data from 24.04.2015–17.10.2019		TCCON station	https://tccondata.org/ (accessed on 16 August 2021) https://tccon-wiki.caltech.edu/Main/TCCONSites (accessed on 16 August 2021)

Table A6. Tall towers in the NOAA Earth System Research Laboratory's Global Greenhouse Gas Reference Network [176].

No.	Name	Location	Coordination	Surface Elevation	Intake Height	Carbon Dioxide Measurement Period	Note
1	Argyle, Maine Tower (AMT)	Argyle, Maine	45.03° N, 68.68° W	50 m a.s.l.	12, 30, 107 m above ground	2003-ongoinssg	
2	Boulder Atmospheric Observatory (BAO)	Erie, Colorado	40.05° N, 105.01° W	1584 m a.s.l.	22, 100, 300 m above ground	2007–2016	Discontinued
3	Barrow Observatory (BRW)	Barrow, Alaska	71.323° N, 156.6114° W	11 m a.s.l.	16.46 m above ground	1971-ongoing	
4	WITN Tower (ITN)	Grifton, North Carolina	5.53° N, 77.38° W	9 m a.s.l.	51, 123, 496 m above ground	1992–1999	Discontinued
5	WLEF Tower (LEF)	Park Falls, Wisconsin	45.9451° N, 90.2732° W	472 m a.s.l.	1, 30, 76, 122, 244, 396 m above ground	2003-ongoing	
6	Mount Bachelor Observatory (MBO)	Mount Bachelor, Oregon	43.9775° N, 121.6861° W	2731 m a.s.l.	11 m above ground	2011-ongoing 2012-ongoing	

Table A6. *Cont.*

No.	Name	Location	Coordination	Surface Elevation	Intake Height	Carbon Dioxide Measurement Period	Note
7	Mauna Loa Observatory (MLO)	Mauna Loa, Hawaii	19.5362° N, 155.5763° W	3397 m a.s.l.	40 m above ground	1969-ongoing	
8	South Carolina Tower (SCT)	Beech Island, South Carolina	33.406° N, 81.833° W	115 m a.s.l.	30, 61, 305 m above ground	2008-ongoing	
9	American Samoa Observatory (SMO)	Tutuila Island, American Samoa	14.2474° S, 170.5644° W	42 m a.s.l.	18 m above ground	1972-ongoing	
10	Shenandoah National Park (SNP)	Shenandoah National Park, Virginia	38.617° N, 78.35° W	1008 m a.s.l.	5, 10, 17 m above ground	2008-ongoing	
11	South Pole Observatory (SPO)	South Pole, Antarctica	89.98° S, 24.8° W	2810 m a.s.l.	11 m above ground	1975-ongoing	
12	West Branch, Iowa (WBI)	West Branch, Iowa	41.725° N, 91.353° W	242 m a.s.l.	31, 99, 379 m above ground	2007-ongoing	
13	Walnut Grove, California (WGC)	Walnut Grove, California	38.265° N, 121.4911° W	0 m a.s.l.	30, 91, 483 m above ground	2007-ongoing	
14	WKT Tower (WKT)	Moody, Texas	31.32° N, 97.33° W	251 m a.s.l.	30, 122, 457 m above ground	2003-ongoing	

References

1. Brovkin, V.; Lorenz, S.; Raddatz, T.; Ilyina, T.; Stemmler, I. What was the source of the atmospheric CO_2 increase during the Holocene? *Biogeosciences* **2019**, *16*, 2543–2555. [CrossRef]
2. Pearman, G.I.; Etheridge, D.; Silva, F.d.; Fraser, P.J. Evidence of changing concentrations of atmospheric CO_2, N_2O and CH_4 from air bubbles in Antarctic ice. *Nature* **1986**, *320*, 248–250. [CrossRef]
3. Yue, T.; Zhang, L.; Zhao, M.; Wang, Y.; Wilson, J. Space-and ground-based CO_2 measurements: A review. *Sci. China Earth Sci.* **2016**, *59*, 2089–2097. [CrossRef]
4. Pieter Tans, and Ralph Keeling, Global Monitoring Laboratory, NOAA/GML. Available online: www.esrl.noaa.gov/gmd/ccgg/trends/ (accessed on 10 February 2021).
5. McElwain, J.; Montañez, I.; White, J.; Wilson, J.; Yiotis, C. Was atmospheric CO_2 capped at 1000 ppm over the past 300 million years? *Palaeogeogr. Palaeoclimatol. Palaeoecol.* **2016**, *441*, 653–658. [CrossRef]
6. Steinthorsdottir, M.; Vajda, V. Early Jurassic (late Pliensbachian) CO_2 concentrations based on stomatal analysis of fossil conifer leaves from eastern Australia. *Gondwana Res.* **2015**, *27*, 932–939. [CrossRef]
7. Goldberg, F. Rate of Increasing Concentrations of Atmospheric Carbon Dioxide Controlled by Natural Temperature Variations. *Energy Environ.* **2008**, *19*, 995–1011. [CrossRef]
8. Fraser, P.J.; Pearman, G.I.; Hyson, P. The Global Distribution of Atmospheric Carbon Dioxide 2. A Review of Provisional Background Observations, 1978–1980. *J. Geophys. Res.* **1983**, *88*, 3591–3598. [CrossRef]
9. Friedlingstein, P.; Jones, M.W.; O'Sullivan, M.; Andrew, R.M.; Hauck, J.; Peters, G.P.; Peters, W.; Pongratz, J.; Sitch, S.; Quéré, C.L.; et al. Global Carbon Budget 2019. *Earth Syst. Sci. Data* **2019**, *11*, 1783–1838. [CrossRef]
10. Jiang, X.; Yung, Y.L. Global Patterns of Carbon Dioxide Variability from Satellite Observations. *Annu. Rev. Earth Planet. Sci.* **2019**, *47*, 225–245. [CrossRef]
11. NOAA. Carbon Cycle Greenhouse Gases. Available online: https://www.esrl.noaa.gov/gmd/ccgg/ (accessed on 10 February 2021).
12. TCCON. Available online: https://tccondata.org/ (accessed on 22 May 2020).
13. CONTRAIL. Available online: https://www.cger.nies.go.jp/contrail/index.html (accessed on 10 February 2021).
14. Singh, H.B.; Jacob, D.; Pfister, L.; Hipskind, R.S. *INTEX-NA: Intercontinental Chemical Transport Experiment—North America*; NASA Ames Research Center: Moffett Field, CA, USA, 2001.
15. NCAR Earth Observing Laboratory. HIAPER Pole-to-Pole Observation. Available online: https://www.eol.ucar.edu/field_projects/hippo-1 (accessed on 10 February 2021).
16. LAGOS. In-Service Aircraft for a Global Observing System. Available online: https://www.iagos.org/ (accessed on 10 February 2021).
17. NASA. Carbon in Arctic Reservoirs Vulnerability Experiment (CARVE). Available online: https://carve.ornl.gov/ (accessed on 10 February 2021).
18. NCEI (NOAA National Centers for Environmental Information). Ships Of Opportunity Program (SOOP) Data. Available online: https://www.ncei.noaa.gov/access/ocean-carbon-data-system/oceans/VOS_Program/ (accessed on 17 February 2021).
19. Takahashi, T.; Sutherland, S.C.; Kozyr, A.; NCEI (NOAA National Centers for Environmental Information). Global Surface pCO2 (LDEO) Database V2019. 2020. Available online: https://www.ncei.noaa.gov/access/ocean-carbon-data-system/oceans/LDEO_Underway_Database/ (accessed on 17 February 2021).
20. Sutton, A.; Sabine, C.; Mathis, J.; Kozyr, A.; Carbon Dioxide Information Analysis Center, Oak Ridge National Laboratory, US Department of Energy. Available online: https://www.ncei.noaa.gov/access/ocean-carbon-data-system/oceans/Moorings/ndp092.html (accessed on 10 February 2021).
21. Pan, G.; Xu, Y.; Ma, J. The potential of CO_2 satellite monitoring for climate governance: A review. *J. Environ. Manag.* **2021**, *277*, 111423. [CrossRef]
22. NASA. Orbiting Carbon Observatory-3. Available online: https://ocov3.jpl.nasa.gov/ (accessed on 10 February 2021).
23. NASA. Orbiting Carbon Observatory-2. Available online: https://earth.esa.int/eogateway/missions/gosat (accessed on 10 February 2021).
24. European Space Agency. GOSAT. Available online: https://earth.esa.int/eogateway/missions/gosat (accessed on 10 February 2021).
25. NASA. TES Get Data. Available online: https://tes.jpl.nasa.gov/data/ (accessed on 10 February 2021).
26. NASA. AIRS Atmospheric Infrared Sounder. Available online: https://airs.jpl.nasa.gov/data/get-data/standard-data/ (accessed on 10 February 2021).
27. NOAA. NOAA Comprehensive Large Array-Data Stewardship System (Class). Available online: https://www.avl.class.noaa.gov/saa/products/search?datatype_family=IASI (accessed on 10 February 2021).
28. eoPortal Directory. SciSat-1/ACE (Science Satellite/Atmospheric Chemistry Experiment). Available online: https://directory.eoportal.org/web/eoportal/satellite-missions/s/scisat-1 (accessed on 10 February 2021).
29. SCHIAMACHY. Available online: https://www.sciamachy.org/ (accessed on 10 February 2021).
30. NOAA. ESRL Global Monitoring Division—Mauna Loa Observatory. Available online: https://www.esrl.noaa.gov/gmd/obop/mlo/ (accessed on 10 February 2021).
31. Wunch, D.; Toon, G.C.; Blavier, J.-F.L.; Washenfelder, R.A.; Notholt, J.; Connor, B.J.; Griffith, D.W.T.; Sherlock, V.; Wennberg, P.O. The total carbon column observing network. *Philos. Trans. A Math Phys. Eng. Sci.* **2011**, *369*, 2087–2112. [CrossRef] [PubMed]

32. Bakwin, P.S.; Tans, P.P.; Zhao, C.; Ussler, W., III; Quesnell, E. Measurements of carbon dioxide on a very tall tower. *Tellus* **1995**, *47B*, 535–549. [CrossRef]
33. Bakwin, P.S.; Tans, P.P.; Hurst, D.F.; Zhao, C. Measurements of carbon dioxide on very tall towers: Results of the NOAA/CMDL program. *Tellus B* **1998**, *50*, 401–415. [CrossRef]
34. NOAA. Measuring & Analyzing Greenhouse Gases: Behind the Scenes. Available online: https://www.esrl.noaa.gov/gmd/ccgg/behind_the_scenes/towers.html (accessed on 10 February 2021).
35. Machida, T.; Matsueda, H.; Sawa, Y.; Nakagawa, Y.; Hirotani, K.; Kondo, N.; Goto, K.; Nakazawa, T.; Ishikawa, K.; Ogawa, T. Worldwide Measurements of Atmospheric CO_2 and Other Trace Gas Species Using Commercial Airlines. *J. Atmos. Ocean. Technol.* **2008**, *25*, 1744–1754. [CrossRef]
36. Avissar, R.; Holder, H.E.; Abehserra, N.; Bolch, M.A.; Novick, K. The Duke University Helicopter Observation Platform. *Bull. Amer. Meteor. Soc.* **2009**, *90*, 939–954. [CrossRef]
37. Ouchi, M.; Masumi, Y.; Nakayama, T.; Shimizu, K.; Sawada, T. Development of a balloon-borne instrument for CO_2 vertical profile observations in the troposphere. *Atmos. Meas. Tech.* **2019**, *12*, 5639–5653. [CrossRef]
38. Bischof, W. Carbon Dioxide Measurements from Aircraft. *Tellus* **1970**, *22*, 545–549. [CrossRef]
39. Hou, Y.; Wang, S.; Zhou, Y.; Yan, F.; Zhu, J. Analysis of the carbon dioxide concentration in the lowest atmospheric layers and the factors affecting China based on satellite observations. *Int. J. Remote Sens.* **2012**, *34*, 1981–1994. [CrossRef]
40. Ota, Y.; Imasu, R. CO_2 Retrieval Using Thermal Infrared Radiation Observation by Interferometric Monitor for Greenhouse Gases (IMG) Onboard Advanced Earth Observing Satellite (ADEOS). *J. Meteorol. Soc. Jpn.* **2016**, *471-490*. [CrossRef]
41. Wunch, D.; Wennberg, P.O.; Osterman, G.; Fisher, B.; Naylor, B. Comparisons of the Orbiting Carbon Observatory-2 (OCO-2) XCO_2 measurements with TCCON. *Atmos. Meas. Tech.* **2017**, *10*, 2209–2238. [CrossRef]
42. Bi, Y.; Wang, Q.; Yang, Z.; Chen, J.; Bai, W. Validation of Column-Averaged Dry-Air Mole Fraction of CO_2 Retrieved from OCO-2 Using Ground-Based FTS Measurements. *J. Meteorol. Res.* **2018**, *32*, 433–443. [CrossRef]
43. Timofeyev, Y.M.; Berezin, I.A.; Virolainen, Y.A.; Makarova, M.V.; Polyakov, A.V.; Poberovsk, A.V. Spatial–Temporal CO2 Variations near St. Petersburg Based on Satellite and Ground-Based Measurements. *Atmos. Ocean. Phys.* **2019**, *55*, 59–64. [CrossRef]
44. Wu, L.; Hasekamp, O.; Hu, H.; De Brugh, J.A.; Landgraf, J.; Butz, A.; Aben, I. Full-physics carbon dioxide retrievals from the Orbiting Carbon Observatory-2 (OCO-2) satellite by only using the 2.06 µm band. *Atmos. Meas. Tech.* **2019**, *12*, 6049–6058. [CrossRef]
45. O'Dell, C.W.; Eldering, A.; Wennberg, P.O.; Crisp, D.; Gunson, M.R.; Fisher, B.; Frankenberg, C.; Kiel, M.; Lindqvist, H.; Mandrake, L.; et al. Improved retrievals of carbon dioxide from Orbiting Carbon Observatory-2 with the version 8 ACOS algorithm. *Atmos. Meas. Tech.* **2018**, *11*, 6539–6576. [CrossRef]
46. Ailin, L.; Ge, H.; Wei, G.; Jie, Y.; Chengzhi, X. Comparison of Global XCO2 Concentrations From OCO-2 With TCCON Data in Terms of Latitude Zones. *IEEE J. Sel. Top. Appl. Earth Obs. Remote Sens.* **2017**, *10*, 2491–2498.
47. Liang, A.; Han, G.; Xu, H.; Gong, W.; Zhang, T. Evaluation of XCO2 from OCO-2 Lite File Product compared with TCCON data. *Int. Geosci. Remote Sens. Symp. IGARSS* **2017**, *8127389*, 2070–2073.
48. Qin, X.C.; Nakayama, T.; Matsumi, Y.; Kawasaki, M.; Imasu, R.; Morino, I.; Tanaka, Y.; Ishidoya, S.; Sato, K.; Ohashi, M. Observation of column-averaged molar mixing ratios of carbon dioxide in Tokyo. *Atmos. Environ. X* **2019**, *2*, 100022.
49. Dan-dan, L.I.U.; Yin-bo, H.U.A.N.G.; Zhen-song, C.A.O.; Xing-ji, L.U.; Yu-song, S.U.N.; Qian-si, T.U. Analysis of Total Columns of Greenhouse Gas Based on Direct Observation and Comparison with Satellite Data in Hefei. *Acta Photonica Sin.* **2020**, *49*, 0301002. [CrossRef]
50. Velazco, V.A.; Deutscher, N.M.; Morino, I.; Uchino, O.; Bukosa, B. Satellite and ground-based measurements of XCO2 in a remote semiarid region of Australia. *Earth Syst. Sci. Data* **2019**, *11*, 935–946. [CrossRef]
51. Eguchi, N.; Yoshida, Y.; Morino, I.; Kikuchi, N.; Saeki, T. Seasonal variations of greenhouse gas column-averaged dry air mole fractions retrieved from swir spectra of gosat tanso-fts. In Proceedings of the 2011 IEEE International Geoscience and Remote Sensing Symposium (IGRASS), Vancouver, BC, Canada, 24–29 July 2011; pp. 3542–3545. [CrossRef]
52. Ohyama, H.; Kawakami, S.; Tanaka, T.; Morino, I.; Uchino, O. Observations of XCO2 and XCH4 with ground-based high-resolution FTS at Saga, Japan, and comparisons with GOSAT products. *Atmos. Meas. Tech.* **2015**, *8*, 5263–5276. [CrossRef]
53. Rokotyan, N.V.; Imasu, R.; Zakharov, V.I.; Gribanov, K.G.; Khamatnurova, M.Y. The Amplitude of the CO2 Seasonal Cycle in the Atmosphere of the Ural Region Retrieved from Ground—Based and Satellite Near—IR Measurements. *Atmos. Ocean. Opt.* **2015**, *28*, 49–55. [CrossRef]
54. Yates, E.L.; Schiro, K.; Lowenstein, M.; Sheffner, E.J.; Iraci, L.T. Carbon Dioxide and Methane at a Desert Site—A Case Study at Railroad Valley Playa, Nevada, USA. *Atmosphere* **2011**, *2*, 702–714. [CrossRef]
55. Qu, Y.; Zhang, C.; Wang, D.; Tian, P.; Bai, W.; Zhang, X. Comparison of atmospheric CO_2 observed by GOSAT and two ground stations in China. *Int. J. Remote Sens.* **2014**, *34*, 3938–3946. [CrossRef]
56. Zeng, Z.-C.; Lei, L.; Strong, K.; Jones, D.B.; Guo, L. Global land mapping of satellite-observed CO_2 total columns using spatio-temporal geostatistics. *Int. J. Digit. Earth* **2017**, *10*, 426–456. [CrossRef]
57. Wunch, D.; Wennberg, P.O.; Toon, G.C.; Connor, B.J.; Fisher, B.; Osterman, G.B.; Frankenberg, C. A Method for Evaluating Bias in Global Measurements of CO_2 Total Columns from Space. *Atmos. Chem. Phys.* **2011**, *23*, 12317–12337. [CrossRef]

58. Yuan, Y.; Sussmann, R.; Rettinger, M.; Ries, L.; Petermeier, H.; Menzel, A. Comparison of Continuous In-Situ CO_2 Measurements with Co-Located Column-Averaged XCO2 TCCON/Satellite Observations and CarbonTracker Model Over the Zugspitze Region. *Remote Sens.* **2019**, *11*, 2981. [CrossRef]
59. Buchwitz, M.; Reuter, M.; Schneising, O.; Hewson, W.; Detmers, R. Global satellite observations of column-averaged carbon dioxide and methane: The GHG-CCI XCO2 and XCH4 CRDP3 data set. *Remote Sens. Environ.* **2017**, *203*, 276–295. [CrossRef]
60. Buchwitz, M.; Reuter, M.; Schneising, O.; Boesch, H.; Guerlet, S.; Dils, B.; Aben, I.; Armante, R.; Bergamaschi, P.; Blumenstock, T.; et al. The Greenhouse Gas Climate Change Initiative (GHG-CCI): Comparison and quality assessment of near-surface-sensitive satellite-derived CO_2 and CH_4 global data sets. *Remote Sens. Environ.* **2013**, *162*, 344–362. [CrossRef]
61. Miao, R.; Lu, N.; Yao, L.; Zhu, Y.; Wang, J.; Sun, J. Multi-Year Comparison of Carbon Dioxide from Satellite Data with Ground-Based FTS Measurements (2003–2011). *Remote Sens.* **2013**, *5*, 3431–3456. [CrossRef]
62. Moon, Y.S.; Arellano, A.F. The characteristics of tropospheric CO_2 retrieved by AIRS, GOSAT and IASI in East Asia. *Disaster Adv.* **2015**, *8*, 1–13.
63. Zhang, L.; Zhang, X.; Jiang, H. Accuracy comparisons of airs, sciamachy and gosat with ground-based data based on global CO_2 concentration. In Proceedings of the 21st International Conference on Geoinformatics, Kaifen, China, 20–22 June 2013; pp. 1–5.
64. Zhang, L.; Jiang, H.; Zhang, X. Comparison analysis of the global carbon dioxide concentration column derived from sciamachy, airs, and gosat with surface station measurements. *Int. J. Remote Sens.* **2015**, *36*, 1406–1423. [CrossRef]
65. Jiang, X.; Crisp, D.; Olsen, E.T.; Kulawik, S.S.; Miller, C.E. CO_2 annual and semiannual cycles from multiple satellite retrievals and models. *Earth Space Sci.* **2016**, *3*, 78–87. [CrossRef]
66. Reuter, M.; Buchwitz, M.; Schneising, O.; Noël, S.; Bovensmann, H.; Burrows, J.P.; Boesch, H.; Di Noia, A.; Anand, J.; Parker, R.J.; et al. Ensemble-based satellite-derived carbon dioxide and methane column-averaged dry-air mole fraction data sets (2003–2018) for carbon and climate applications. *Atmos. Meas. Tech.* **2020**, *13*, 789–819. [CrossRef]
67. Buchwitz, M.; Reuter, M.; Schneising, O.; Noëll, S.; Gier, B. Computation and analysis of atmospheric carbon dioxide annual mean growth rates from satellite observations during 2003–2016. *Atmos. Chem. Phys.* **2018**, *18*, 17355–17370. [CrossRef]
68. Dils, B.; Buchwitz, M.; Reuter, M.; Schneising, O.; Boesch, H.; Parker, R.; Guerlet, S.; Aben, I.; Blumenstock, T.; Burrows, J.P.; et al. The Greenhouse Gas Climate Change Initiative (GHG-CCI): Comparative validation of GHG-CCI sciamachy/envisat and tanso-fts/gosat CO_2 and CH_4 retrieval algorithm products with measurements from the TCCON. *Atmos. Meas. Tech.* **2014**, *7*, 1723–1744. [CrossRef]
69. Kim, W.; Kim, J.; Jung, Y.; Boesch, H.; Lee, H. Retrieving XCO2 from GOSAT FTS over East Asia Using Simultaneous Aerosol Information from CAI. *Remote Sens.* **2016**, *8*, 994. [CrossRef]
70. Yang, D.; Liu, Y.; Cai, Z.; Deng, J.; Wang, J.; Chen, X. An advanced carbon dioxide retrieval algorithm for satellite measurements and its application to GOSAT observations. *Sci. Bull.* **2015**, *60*, 2063–2066. [CrossRef]
71. Lindqvist, H.; O'Dell, C.W.; Basu, S.; Boesch, H.; Chevallier, F.; Deutscher, N.; Feng, L.; Fisher, B.; Hase, F.; Inoue, M.; et al. Does GOSAT capture the true seasonal cycle of carbon dioxide? *Atmos. Chem. Phys.* **2015**, *15*, 13023–13040. [CrossRef]
72. Yi, Y.; Liu, Y.; Cai, Z.; Fang, S.; Yang, D.; Wang, Y.; Liang, M.; Yan, B.; Ma, Q.; Wang, M. Measuring and comparing in-situ CO_2 and CO profiles with satellite observations and model data. *Atmos. Ocean. Sci. Lett.* **2019**, *12*, 444–450. [CrossRef]
73. Tadić, J.M.; Michalak, A.M. On the effect of spatial variability and support on validation of remote sensing observations of CO_2. *Atmos. Environ.* **2016**, *132*, 309–316. [CrossRef]
74. Maddy, E.S.; Barnet, C.D.; Goldberg, M.; Sweeney, C.; Liu, X. CO_2 retrievals from the Atmospheric Infrared Sounder: Methodology and validation. *J. Geophys. Res. Atmos.* **2008**, *113*, D11301. [CrossRef]
75. Chahine, M.; Barnet, C.; Olsen, E.T.; Chen, L.; Maddy, E. On the determination of atmospheric minor gases by the method of vanishing partial derivatives with application to CO_2. *Geophys. Res. Lett.* **2005**, *32*. [CrossRef]
76. Uspensky, A.B.; Kukharsky, A.V.; Romanov, S.V.; Rublev, A.N. Monitoring the Carbon Dioxide Mixing Ratio in the Troposphere and the Methane Total Column over Siberia According to the Data of the AIRS and IASI IR Sounders. *Atmos. Ocean. Phys.* **2011**, *47*, 1097–1103. [CrossRef]
77. Kukharskii, A.V.; Uspenskii, A.B. Determination of tropospheric mean carbon dioxide concentration from satellite high spectral resolution IR-sounder data. *Russ. Meteorol. Hydrol.* **2009**, *34*, 202–211. [CrossRef]
78. Frankenberg, C.; Kulawik, S.S.; Wofsy, S.C.; Chevallier, F.; Daube, B.; Kort, E.A.; O'dell, C.; Olsen, E.T.; Osterman, G. Using airborne HIAPER Pole-to-Pole Observations (HIPPO) to evaluate model and remote sensing estimates of atmospheric carbon dioxide. *Atmos. Chem. Phys.* **2016**, *16*, 7867–7878. [CrossRef]
79. Glen, S. StatisticsHowTo.com. Available online: https://www.statisticshowto.com/pooled-standard-deviation/ (accessed on 15 January 2021).
80. NASA. GES DISK. Available online: https://disc.gsfc.nasa.gov/datasets/OCO2_L2_Lite_FP_9r/summary (accessed on 10 February 2021).
81. NASA. User's Guide. Available online: https://docserver.gesdisc.eosdis.nasa.gov/public/project/OCO/OCO2_DUG.V9.pdf (accessed on 12 November 2021).
82. Yu, S.; Rosenberg, R.; Bruegge, C.; Chapsky, L.; Fu, D.; Lee, R.; Taylor, T.; Cronk, H.; O'Dell, C.; Angal, A.; et al. Stability Assessment of OCO-2 Radiometric Calibration Using Aqua MODIS as a Reference. *Remote Sens.* **2020**, *12*, 1269. [CrossRef]
83. NASA. Available online: https://ocov2.jpl.nasa.gov/observatory/instrument/ (accessed on 11 November 2021).

84. NASA. GES DISK Documentation. Available online: https://docserver.gesdisc.eosdis.nasa.gov/public/project/OCO/OCO2_OCO3_B10_DUG.pdf (accessed on 10 February 2021).
85. Pearman, G.I.; Hyson, P.; Fraser, P.J. The global distribution of atmospheric carbon dioxide: 1 Aspects of observations and modeling. *J. Geophys. Res.* **1983**, *88*, 3581–3590. [CrossRef]
86. Trenberth, K.E.; Guillemot, C.J. The total mass of the atmosphere. *J. Geophys. Res.* **1994**, *99*, 23079–23088. [CrossRef]
87. Trenberth, K.E.; Smith, L. The Mass of the Atmosphere: A Constraint on Global Analyses. *J. Clim.* **2005**, *18*, 864–875. [CrossRef]
88. Müller, A.; Tanimoto, H.; Sugita, T.; Machida, T.; Nakaoka, S.-I.; Patra, P.K.; Laughner, J.; Crisp, D. New approach to evaluate satellite derived XCO2 over oceans by integrating ship and aircraft observations. *Atmos. Chem. Phys.* **2021**, *21*, 8255–8271. [CrossRef]
89. Prasad, P.; Rastogi, S.; Singh, R. Study of satellite retrieved CO_2 and CH_4 concentration over India. *Adv. Space Res.* **2014**, *54*, 1933–1940. [CrossRef]
90. Rossi, F.S.; Santos, G.A.D.A.; Maria, L.D.S.; Lourençoni, T.; Pelissari, T.D.; Della-Silva, J.L.; Júnior, J.W.O.; Silva, A.d.A.e.; Lima, M.; Teodoro, P.E.; et al. Carbon dioxide spatial variability and dynamics for contrasting land uses in central Brazil agricultural frontier from remote sensing data. *J. S. Am. Earth Sci.* **2022**, *116*, 103809. [CrossRef]
91. Patil, M.N.; Dharmaraj, T.; Waghmare, R.T.; Singh, S.; Pithani, P.; Kulkarni, R.; Dhangar, N.; Siingh, D.; Chinthalu, G.R.; Singh, R.; et al. Observations of carbon dioxide and turbulent fluxes during fog conditions in north India. *J. Earth Syst. Sci.* **2020**, *129*, 51. [CrossRef]
92. Li, Y.; Zhang, C.; Li, F. Influence of thin cirrus clouds on the short-wave infrared satellite observation of atmospheric CO2. *Opt. Int. J. Light Electron Opt.* **2019**, *208*, 164140. [CrossRef]
93. Siabi, Z.; Falahatkar, S.; Alavi, S.J. Spatial distribution of XCO2 using OCO-2 data in growing seasons. *J. Environ. Manag.* **2019**, *244*, 110–118. [CrossRef]
94. Ivakhov, V.M.; Paramonova, N.N.; Privalov, V.I.; Zinchenko, A.V.; Loskutova, M.A.; Makshtas, A.P.; Kustov, V.Y.; Laurila, T.; Aurela, M.; Asmi, E. Atmospheric Concentration of Carbon Dioxide at Tiksi and Cape Baranov Stations in 2010–2017. *Russ. Meteorol. Hydrol.* **2019**, *44*, 291–299. [CrossRef]
95. Al-jaf, S.J.; Al-Taai, O.T. Impact of carbon dioxide concentrations on atmospheric temperature changes over iraq and some neighboring countries. *Plant Arch.* **2019**, *19*, 1450–1456.
96. Xueref-Remy, I.; Dieudonné, E.; Vuillemin, C.; Lopez, M.; Lac, C.; Schmidt, M.; Delmotte, M.; Chevallier, F.; Ravetta, F.; Perrussel, O.; et al. Diurnal, synoptic and seasonal variability of atmospheric CO_2 in the Paris megacity area. *Atmos. Chem. Phys.* **2018**, *18*, 3335–3362. [CrossRef]
97. Pathakoti, M.; Gaddamidi, S.; Gharai, B.; Syamala, P.S.; Rao, P.V. Influence of meteorological parameters on atmospheric CO_2 at Bharati, the Indian Antarctic research station. *Polar Res.* **2018**, *37*, 1442072. [CrossRef]
98. Yin, S.; Wang, X.; Tani, H.; Zhang, X.; Zhong, G. Analyzing temporo-spatial changes and the distribution of the CO2 T concentration in Australia from 2009 to 2016 by greenhouse gas monitoring satellites. *Atmos. Environ.* **2018**, *192*, 1–12. [CrossRef]
99. Bie, N.; Lei, L.; Zeng, Z.; Cai, B.; Yang, S. Regional uncertainty of GOSAT XCO2 retrievals in China: Quantification and attribution. *Atmos. Meas. Tech.* **2018**, *11*, 1251–1272. [CrossRef]
100. Ge, H.; Hao, X.; Wei, G.; Jiqiao, L.; Juan, D. Feasibility Study on Measuring Atmospheric CO_2 in Urban Areas Using Spaceborne CO2-IPDA LIDAR. *Remote Sensig* **2018**, *10*, 985.
101. Jiang, X.; Kao, A.; Corbett, A.; Olsen, E.; Pagano, T.; Zhai, A.; Newman, S.; Li, L.; Yung, Y. Influence of Droughts on Mid-Tropospheric CO_2. *Remote Sens.* **2017**, *9*, 852. [CrossRef]
102. Mousavi, S.M.; Falahatkar, S.; Farajzadeh, M. Assessment of seasonal variations of carbon dioxide concentration in Iran using GOSAT data. *Nat. Resour. Forum* **2017**, *41*, 83–91. [CrossRef]
103. Falahatkar, S.; Mousavi, S.M.; Farajzadeh, M. Spatial and temporal distribution of carbon dioxide gas using GOSAT data over IRAN. *Environ. Monit. Assess.* **2017**, *189*, 627. [CrossRef] [PubMed]
104. Lei, L.; Zhong, H.; He, Z.; Cai, B.; Yang, S.; Wu, C.; Zeng, Z.; Liu, L.; Zhang, B. Assessment of atmospheric CO_2 concentration enhancement from anthropogenic emissions based on satellite observations. *Chin. J.* **2017**, *62*, 2941–2950.
105. Hedelius, J.K.; Feng, S.; Roehl, C.M.; Wunch, D.; Hillyard, P.W. Emissions and topographic effects on column CO_2 (X CO2) variations, with a focus on the Southern California Megacity. *J. Geophys. Res. Atmos.* **2017**, *122*, 7200–7215. [CrossRef]
106. Esteki, K.; Prakash, N.; Li, Y.; Mu, C.; Du, K. Seasonal Variation of CO_2 Vertical Distribution in the Atmospheric Boundary Layer and Impact of Meteorological Parameters. *Int. J. Environ. Res.* **2017**, *11*, 707–721. [CrossRef]
107. Pan, C.; Zhu, X.; Wei, N.; Zhu, X.; She, Q. Spatial variability of daytime CO_2 concentration with landscape structure across urbanization gradients, Shanghai, China. *Clim. Res.* **2016**, *69*, 107–116. [CrossRef]
108. Taylor, T.E.; O'Dell, C.W.; Frankenberg, C.; Partain, P.T.; Cronk, H.Q. Orbiting Carbon Observatory-2 (OCO-2) cloud screening algorithms: Validation against collocated MODIS and CALIOP data. *Atmos. Meas. Tech.* **2016**, *9*, 973–989. [CrossRef]
109. Jung, Y.; Kim, J.; Kim, W.; Lee, H.B. Impact of Aerosol Property on the Accuracy of a CO_2 Retrieval Algorithm from Satellite Remote Sensing. *Remote Sens.* **2016**, *8*, 322. [CrossRef]
110. Hernández-Paniagua, I.Y.; Lowry, D.; Clemitshaw, K.C.; Fisher, R.E.; France, J.L.; Lanoisellé, M.; Ramonet, M.; Nisbet, E.G. Diurnal, seasonal, and annual trends in atmospheric CO_2 at southwest London during 2000–2012: Wind sector analysis and comparison with Mace Head, Ireland. *Atmos. Environ.* **2015**, *105*, 138–147. [CrossRef]

111. Liu, M.; Wu, J.; Zhu, X.; He, H.; Jia, W.; Xiang, W. Evolution and variation of atmospheric carbon dioxide concentration over terrestrial ecosystems as derived from eddy covariance measurements. *Atmos. Environ.* **2015**, *114*, 75–82. [CrossRef]
112. Liu, X.M.; Cheng, X.L.; Hu, F. Gradient characteristics of CO_2 concentration and flux in Beijing urban area part I: Concentration and virtual temperature. *Chin. J. Geophys. Chin. Ed.* **2015**, *17*, 501–511.
113. Gratani, L.; Varone, L. Atmospheric carbon dioxide concentration variations in Rome: Relationship with traffic level and urban park size. *Urban Ecosyst.* **2014**, *17*, 501–511. [CrossRef]
114. Park, M.-S.; Joo, S.J.; Park, S.-U. Carbon dioxide concentration and flux in an urban residential area in Seoul, Korea. *Adv. Atmos. Sci.* **2014**, *31*, 1101–1112. [CrossRef]
115. Fang, S.X.; Zhou, L.X.; Tans, P.P.; Ciais, P.; Steinbacher, M.; Xu, L.; Luan, T. In situ measurement of atmospheric CO_2 at the four WMO/GAW stations in China. *Atmos. Chem. Phys.* **2014**, *14*, 2541–2554. [CrossRef]
116. Retrieval and analysis of atmospheric XCO2 using ground-based spectral observation. *Guang Pu Xue Yu Guang Pu Fen Xi/Spectrosc. Spectr. Anal.* **2014**, *34*, 1729–1735.
117. Li, Y.; Deng, J.; Mu, C.; Xing, Z.; Du, K. Vertical distribution of CO_2 in the atmospheric boundary layer: Characteristics and impact of meteorological variables. *Atmos. Environ.* **2014**, *91*, 110–117. [CrossRef]
118. Górka, M.; Lewicka-Szczebak, D. One-year spatial and temporal monitoring of concentration and carbon isotopic composition of atmospheric CO_2 in a Wrocław (SW Poland) city area. *Appl. Geochem.* **2013**, *35*, 7–13. [CrossRef]
119. Li, Y.L.; Mu, C.; Deng, J.J.; Zhao, S.H.; Du, K. Near surface atmospheric CO_2 variations in autumn at suburban Xiamen, China. *Huanjing Kexue/Environ. Sci.* **2013**, *34*, 2018–2024.
120. Büns, C.; Kuttler, W. Path-integrated measurements of carbon dioxide in the urban canopy layer. *Atmos. Environ.* **2012**, 237–247. [CrossRef]
121. Wu, J.; Guan, D.; Yuan, F.; Yang, H.; Wang, A.; Jin, C. Evolution of atmospheric carbon dioxide concentration at different temporal scales recorded in a tall forest. *Atmos. Environ.* **2012**, *61*, 9–14. [CrossRef]
122. García, M.A.; Sánchez, M.L.; Pérez, I.A. Differences between carbon dioxide levels over suburban and rural sites in Northern Spain. *Environ. Sci. Pollut. Res.* **2012**, *19*, 432–439. [CrossRef]
123. Yanfang, H.; Shixin, W.; Yi, Z.; Feng, W.; Wenliang, L.; Yu, H. Variations of Greenhouse Gas carbon dioxide concentration over the Chinese mainland based on Satellite and Background Measurements. *Disaster Adv.* **2012**, *5*, 871–876.
124. Bostrom, A.R. Measurements of carbon dioxide in an Oregon metropolitan region. *Atmos. Environ.* **2011**, *45*, 1138–1144.
125. Ramamurthy, P.; Pardyjak, E.R. Toward understanding the behaviour of carbon dioxide and surface energy fluxes in the urbanized semi-arid Salt Lake Valley, Utah, USA. *Atmos Environ.* **2011**, *45*, 73–84. [CrossRef]
126. Xueref-Remy, I.; Messager, C.; Filippi, D.; Pastel, M.; Nedelec, P.; Ramonet, M.; Paris, J.D.; Ciais, P. Variability and budget of CO_2 in Europe: Analysis of the CAATER airborne campaigns—Part 1: Observed variability. *Atmos. Chem. Phys.* **2011**, *11*, 5655–5672. [CrossRef]
127. Wang, K.; Jiang, H.; Zhang, X.; Zhou, G. Analysis of spatial and temporal variations of carbon dioxide over China using SCIAMACHY satellite observations during 2003–2005. *Int. J. Remote Sens.* **2011**, *32*, 815–832. [CrossRef]
128. Yoshida, Y.; Ota, Y.; Eguchi, N.; Kikuchi, N.; Nobuta, K.; Tran, H.; Morino, I.; Yokota, T. Retrieval algorithm for CO_2 and CH_4 column abundances from short-wavelength infrared spectral observations by the Greenhouse gases observing satellite. *Atmos. Meas. Tech.* **2011**, *4*, 717–734. [CrossRef]
129. Sirignano, C.; Neubert, R.E.; Rödenbeck, C.; Meijer, H.A. Atmospheric oxygen and carbon dioxide observations from two European coastal stations 2000–2005: Continental influence, trend changes and APO climatology. *Atmos. Chem. Phys.* **2010**, *10*, 1599–1615. [CrossRef]
130. Gurk, C.; Fischer, H.; Hoor, P.; Lawrence, M.G.; Lelieveld, J.; Wernli, H. Airborne in-situ measurements of vertical, seasonal and latitudinal distributions of carbon dioxide over Europe. *Atmos. Chem. Phys.* **2008**, *8*, 6395–6403. [CrossRef]
131. George, K.; Ziska, L.H.; Bunce, J.A.; Quebedeauxb, B. Elevated atmospheric CO_2 concentration and temperature across an urban–rural transect. *Atmos. Environ.* **2007**, *41*, 7654–7665. [CrossRef]
132. Aben, I.; Hasekamp, O.; Hartmann, W. Uncertainties in the space-based measurements of CO_2 columns due to scattering in the Earth's atmosphere. *J. Quant. Spectrosc. Radiat. Transf.* **2007**, *104*, 450–459. [CrossRef]
133. Yang, Y.; Tan, J.; Zheng, Y.; Cheng, S. Study on the atmospheric stabilities and the thickness of atmospheric mixed layer during recent 15 years in Shanghai. *Sci. Meteorol. Sin.* **2006**, *26*, 536–541.
134. Gratani, L.; Varone, L. Daily and seasonal variation of CO_2 in the city of Rome in relationship with the traffic volume. *Atmos. Environ.* **2005**, *39*, 2619–2624. [CrossRef]
135. Nasrallah, H.A.; Balling, R.C., Jr.; Madi, S.M.; Al-Ansari, L. Temporal variations in atmospheric CO_2 concentrations in Kuwait City, Kuwait with comparisons to Phoenix, Arizona, USA. *Environ. Pollut.* **2003**, *121*, 301–305. [CrossRef]
136. Chamard, P.; Thiery, F.; Sarra, A.D.; Ciattaglia, L.; Silvestri, L.D. Interannual variability of atmospheric CO_2 in the Mediterranean: Measurements at the island of Lampedusa. *Tellus* **2003**, *55B*, 83–93. [CrossRef]
137. Yuesi, W.; Changke, W.; Xueqing, G.; Guangren, L.; Yao, H. Trend, seasonal and diurnal variations of atmospheric CO_2 in Beijing. *Chin. Sci. Bull.* **2002**, *47*, 2050–2055.
138. Wentz, E.A.; Gober, P.; Balling, R.C., Jr.; Day, T.A. Spatial Patterns and Determinants of Winter Atmospheric Carbon Dioxide Concentrations in an Urban Environment. *Ann. Assoc. Am. Geogr.* **2002**, *92*, 15–28. [CrossRef]

139. Engelen, R.J.; Denning, A.S.; Gurney, K.R.; Stephen, G.L. Global observations of the carbon budget 1 Expected satellite capabilities for emission spectroscopy in the EOS and NPOESS eras. *J. Geophys. Res.* **2001**, *106*, 20055–20068. [CrossRef]
140. Conway, T.J.; Tans, P.; Waterman, L.S.; Thoning, K.W.; Masarie, K.A.; Gammon, R.H. Atmospheric carbon dioxide measurements in the remote global troposphere, 1981–1984. *Tellus B Chem. Phys. Meteorol.* **1988**, *40*, 81–115. [CrossRef]
141. NOAA. Global Monitoring Laboratory. Available online: https://www.esrl.noaa.gov/gmd/dv/site/index.php?program=ccgg (accessed on 10 February 2021).
142. Deng, A.J.; Guo, H.B.; Hu, J.; Jiang, C.Z.; Liu, P.G.; Jing, H.F. Temporal and distribution characteristic of CO_2 concentration over China based on GOSAT satellite data. *J. Remote Sens.* **2020**, *24*, 319–325.
143. Kong, Y.; Chen, B.; Measho, S. Spatio-Temporal Consistency Evaluation of XCO2 Retrievals from GOSAT and OCO-2 Based on TCCON and Model Data for Joint Utilization in Carbon Cycle Research. *Atmosphere* **2019**, *10*, 354. [CrossRef]
144. Wu, L.; Hasekamp, O.; Hu, H.; Landgraf, J.; Butz, A. Carbon dioxide retrieval from OCO-2 satellite observations using the RemoTeC algorithm and validation with TCCON measurements. *Atmos. Meas. Tech.* **2018**, *11*, 3111–3130. [CrossRef]
145. Velazco, V.A.; Morino, I.; Uchino, O.; Hori, A.; Kie, M. TCCON Philippines: First Measurement Results, Satellite Data and Model Comparisons in Southeast. *Asia Remote Sens.* **2017**, *9*, 1228. [CrossRef]
146. Ailin, L.; Wei, G.; Ge, H.; Chengzhi, X. Comparison of Satellite-Observed XCO2 from GOSAT, OCO-2, and Ground-Based TCCON. *Remote Sens.* **2017**, *9*, 1033.
147. Chisa, I.; Ryoichi, I.; Andrey, B.; Tatsuya, Y.; Yukio, Y. Validation of GOSAT SWIR XCO2 and XCH4 Retrieved by PPDF-S Method and Comparison with Full Physics Method. *Sci. Online Lett. Atmos.* **2017**, *13*, 168–173.
148. Liang, A.; Gong, W.; Han, G. OCO-2 XCO2 validation using TCCON data. *Int. Geosci. Remote Sens. Symp. IGARSS* **2016**, *7729210*, 830–833.
149. Kulawik, S.; Wunch, D.; O'Dell, C.; Frankenberg, C.; Reuter, M. Consistent evaluation of ACOS-GOSAT, BESD-SCIAMACHY, CarbonTracker, and MACC through comparisons to TCCON. *Atmos. Meas. Tech.* **2016**, *9*, 683–709. [CrossRef]
150. Anjian, D.; Tao, Y.; Tianhai, C.; Xingfa, G.; Fengjie, Z.; Hong, G. Intercomparison of Carbon Dioxide Products Retrieved from GOSAT Short-Wavelength Infrared Spectra for Three Years (2010–2012). *Atmosphere* **2016**, *7*, 109.
151. Zhou, M.; Dils, B.; Wang, P.; Detmers, R.; Yoshida, Y. Validation of TANSO-FTS/GOSAT XCO2 and XCH4 glint mode retrievals using TCCON data from near-ocean sites. *Atmos. Meas. Tech.* **2016**, *9*, 1415–1430. [CrossRef]
152. Heymann, J.; Reuter, M.; Hilker, M.; Buchwitz, M.; Schneising, O. Consistent satellite XCO2 retrievals from SCIAMACHY and GOSAT using the BESD algorithm. *Atmos. Meas. Tech.* **2015**, *8*, 2961–2980. [CrossRef]
153. Miao, Z.; Xing-Ying, Z.; Rui-Xia, L.; Lie-Qun, H. A study of the validation of atmospheric CO_2 from satellite hyper spectral remote sensing. *Adv. Clim. Chang. Res.* **2014**, *5*, 131–135.
154. Morino, I.; Uchino, O.; Inoue, M.; Yoshida, Y.; Yokota, T. Preliminary validation of column-averaged volume mixing ratios of carbon dioxide and methane retrieved from GOSAT short-wavelength infrared spectra. *Atmos. Meas. Tech.* **2011**, *4*, 1061–1076. [CrossRef]
155. Yoshida, Y.; Kikuchi, N.; Morino, I.; Uchino, O.; Oshchepkov, S. Improvement of the retrieval algorithm for GOSAT SWIR XCO2 and XCH4 and their validation using TCCON data. *Atmos. Meas. Tech.* **2013**, *6*, 1533–1547. [CrossRef]
156. Cogan, A.J.; Boesch, H.; Parker, R.J.; Feng, L.; Palmer, P.I.; Blavier, J.F.; Deutscher, N.M.; Macatangay, R.; Notholt, J.; Roehl, C.; et al. Atmospheric carbon dioxide retrieved from the Greenhouse gases Observing SATellite (GOSAT): Comparison with ground-based TCCON observations and GEOS-Chem model calculations. *J. Geophys. Res. Atmos.* **2012**, *117*, D21. [CrossRef]
157. Butz, A.; Guerlet, S.; Hasekamp, O.; Schepers, D.; Galli, A.; Aben, I.; Frankenberg, C.; Hartmann, J.M.; Tran, H.; Kuze, A.; et al. Toward accurate CO_2 and CH4 observations from GOSAT. *Geophys. Res. Lett.* **2011**, *38*, L14812. [CrossRef]
158. Kasim, O.F.; Abshare, M.W.; Mukuna, T.E.; Wahab, B. Land Use and Ambient Air Quality in Bahir Dar and Hawassa, Ethiopia. *Air Soil Water Res.* **2018**, *11*, 1–10. [CrossRef]
159. Virolainen, Y.A. Methodical aspects of the determination of carbon dioxide in atmosphere using ftir spectroscopy. *J. Appl. Spectrosc.* **2018**, *85*, 462–469. [CrossRef]
160. Wang, W.; Tian, Y.; Liu, C.; Sun, Y.; Liu, W. Investigating the performance of a greenhouse gas observatory in Hefei, China. *Atmos. Meas. Tech.* **2017**, *10*, 2627–2643. [CrossRef]
161. Buschmann, M.; Deutscher, N.M.; Sherlock, V.; Palm, M.; Warneke, T.; Notholt, J. Retrieval of xCO2 from ground-based mid-infrared (NDACC) solar absorption spectra and comparison to TCCON. *Atmos. Meas. Tech.* **2016**, *9*, 577–585. [CrossRef]
162. Gisi, M.; Hase, F.; Dohe, S.; Blumenstock, T.; Simon, A.; Keens, A. XCO2-measurements with a tabletop FTS using solar absorption spectroscopy. *Atmos. Meas. Tech.* **2012**, *5*, 2969–2980. [CrossRef]
163. Yang, Z.; Toon, G.C.; Margolis, J.S.; Wennberg, P.O. Atmospheric CO2 retrieved from ground-based near IR solar spectra. *Geophys. Res. Lett.* **2002**, *29*, 53-1–53-4. [CrossRef]
164. Matsueda, I.H. Variations in Atmospheric CO_2 at the Meteorological Research Institute, Tsukuba, Japan. *J. Atmos. Chem.* **1996**, *23*, 137–161.
165. Cundari, V.; Colombo, T.; Ciattagli, L. Thirteen Years of Atmospheric Carbon Dioxide Measurements at Mt Cimone Station 1995, Italy. *Il Nuovo Cim.* **1995**, *18C*, 33–47. [CrossRef]
166. Navascues, B.; Jardin, C.; Rus, C. Carbon dioxide observations at Izaña baseline station, Tenerife (Canary Islands): 1984–1988. *Tellus B* **1991**, *43*, 118–125. [CrossRef]

167. Gaudry, A.; Monfray, P.; Polian, G.; Bonsang, G.; Ardouin, B.; Jegou, A.; Lambert, G. Non-seasonal variations of atmospheric CO_2 concentrations at Amsterdam Island. *Tellus B Chem. Phys. Meteorol. B* **1991**, *43*, 136–143. [CrossRef]
168. Mook, W.G.; Koopmans, M.; Carter, A.F.; Keeling, C.D. Seasonal, Latitudinal, and Secular Variations in the Abundance and Isotopic Ratios of Atmospheric Carbon Dioxide 1 Results From Land Stations. *J. Geophys. Res.* **1983**, *88*, 10915–10933. [CrossRef]
169. Francey, R.J.; Steele, L.P.; Langenfelds, R.L.; Allison, C.E.; Cooper, L.N. Atmospheric carbon dioxide and its stable isotope ratios, methane, carbon monoxide, nitrous oxide and hydrogen from Shetland Isles. *Atmos. Environ.* **1998**, *32*, 3331–3338. [CrossRef]
170. Schmidt, M.; Graul, R.; Sartorius, H.; Levin, I. The Schauinsland CO_2 record: 30 years of continental observations and their implications for the variability of the European CO_2 budget. *J. Geophys. Res. Atmos.* **2003**, *108*. [CrossRef]
171. Chmura, L.; Rozanski, K.; Necki, J.M.; Zimnoch, M.; Korus, A.; Pycia, M. Atmospheric Concentrations of Carbon Dioxide in Southern Poland: Comparison of Mountain and Urban Environments. *Pol. J. Environ. Stud.* **2008**, *6*, 859–867.
172. Belikov, I.B.; Brenninkmeijer, C.A.; Elansky, N.F.; Ral'ko, A.A. Methane, Carbon Monoxide, and Carbon Dioxide Concentrations Measured in the Atmospheric Surface Layer over Continental Russia in the TROICA Experiments. *Atmos. Ocean. Phys.* **2006**, *42*, 46–59. [CrossRef]
173. Timokhina, A.V.; Prokushkin, A.S.; Onuchin, A.A.; Panov, A.V.; Kofman, G.B. Long-term Trend in CO_2 Concentration in the Surface Atmosphere over Central Siberia. *Russ. Meteorol. Hydrol.* **2015**, *40*, 186–190. [CrossRef]
174. Kozlova, E.A. Methodology and calibration for continuous measurements of biogeochemical trace gas and O_2 concentrations from a 300-m tall tower in central Siberia. *Atmos. Meas. Tech.* **2009**, *2*, 205–220. [CrossRef]
175. Vermeulen, A.T.; Hensen, A.; Popa, M.E.; Bulk, W.C.M.V.D.; Jongejan, P.A.C. Greenhouse gas observations from Cabauw Tall Tower (1992–2010). *Atmos. Meas. Tech.* **2011**, *4*, 617–644. [CrossRef]
176. NOAA. In-Situ Measurement Program. Available online: https://gml.noaa.gov/ccgg/insitu/ (accessed on 10 February 2021).